15
Heterogeneous Multiphase Reactions*

Madhvanand N. Kashid, David W. Agar, Albert Renken, and Lioubov Kiwi-Minsker

15.1
Introduction

Heterogeneous reaction systems can be subdivided into three classes based on the number of phases involved:

- fluid–solid (generally one mobile phase)
- fluid–fluid (generally two mobile phases)
- three-phase reactions (generally two mobile and one fixed phase).

A few examples of such reactions are listed in Table 15.1. The *fluid–solid reactions* are carried out in various types of reactors, such as packed beds, fluidized/slurry and catalytic wall reactors. Packed bed reactors are relatively simple, easy to operate and more suitable for reactions which require relatively large amounts of catalyst, since they provide a high volumetric catalyst fraction of 60–65%. Heat supply/removal and fluid maldistribution are two main drawbacks commonly encountered with such reactors.

The avoidance of hot spot formation during exothermic reactions represents a particular challenge when designing fixed-bed reactors, since it can affect both performance and safety. The importance of considering heat and mass transfer during reactor design is dictated by the chemical reaction kinetics, with fast reactions being more sensitive to physical limitations. Fluidized beds provide an almost isothermal environment for rapid reactions, but only in a narrow operating window. Moreover, such reactors impose special demands on the catalyst and are difficult to scale up. The suspension and retention of the fine solid catalyst make slurry reactors susceptible to similar hydrodynamic constraints. Simply diluting the catalyst in the vicinity of the hot spot is a reliable countermeasure against excessive temperature excursions, but it diminishes space–time yields and fails to exploit the full catalytic potential available. Several original approaches have been adopted to overcome this problem [3].

*A List of Symbols can be found at the end of this chapter.

Micro Process Engineering, Vol.1: Fundamentals, Operations and Catalysts
Edited by V. Hessel, A. Renken, J.C. Schouten, and J.-I. Yoshida

ISBN: 978-3-527-31550-5

Table 15.1 Examples of the conventional multiphase reactions and reactors.

Type of reaction	Reactors	Examples
1. Fluid–solid	Fixed-bed	Synthesis of SO_3 and NO on transition metal oxide or noble metal catalysts
	Fluidized bed	Cracking of hydrocarbons on zeolites
	Slurry	Ethylene oligomerization on sulfated nickel/alumina catalyst
2. Fluid–fluid:	Stirred tank	Chlorination and ozonation
2.1. Gas–liquid	Bubble column	Chlorohydrin process for propylene oxide synthesis
	Spray column	Fertilizer manufacture by acid absorption of dilute NH_3
	Multistage contactor	Soda manufacture
	Packed column	Removal of acid gases from synthesis and natural gas
2.2. Liquid–liquid	Mixer-settler	Nitration
	Centrifugal extractor	Dithiocarbonate synthesis
	Column	Oximation
	Tubular contactor	Fat and ester hydrolysis
3. Three phase:	Packed bed	Catalytic hydrodesulphurization
3.1. Gas–liquid–solid	Fluidized bed	Fischer–Tropsch process
	Slurry	Catalytic hydrogenations
3.2. Gas–liquid–liquid	Stirred tank	Biphasic hydroformylation
	Bubble column	Anthraquinone process for H_2O_2 synthesis

In *fluid–fluid (gas–liquid and liquid–liquid)* systems, a solute usually diffuses from one fluid phase into the other, in which the reaction then takes place. The product may pass back into the first non-reactive phase. In liquid–liquid and some gas–liquid systems, the reaction may actually occur in both phases (e.g. oximation of cyclohexanone [4]). As with heat transfer, rapid reaction kinetics trend to exacerbate mass transfer limitations, especially when only small specific interfacial areas are available. In contrast to the specific surface area for heat transfer, fluid–fluid interfacial areas are dependent on physical properties and operating conditions.

Conventionally, fluid–fluid reactions are carried out in agitated vessels, centrifugal devices, columns (in spray, packed, plate and vibrating varieties) and straight or coiled tubes. The contacting methods involved are bubbling, film formation or dispersive spraying of one fluid into the other.

Three phase reactions comprise gas–liquid–solid and gas–liquid–liquid reactions. Gas–liquid reactions using solid catalysts represent a very important class of reactions. They may be carried out in either slurry (such as bubble column, stirred tank and gas–liquid fluidized configurations) or fixed-bed reactors (trickle bed with co-current-downflow or co-current-upflow, segmented bed and counter-current gas–liquid arrangements).

For gas–liquid–liquid reactions, equipment similar to that used for liquid–liquid extraction is employed. The hydrodynamics in these reactors are extremely

complex due to the three phases and their convoluted interactions. An example is the "grazing" behavior of small solid particles enhancing mass transfer at gas–liquid interfaces. The scale-up from laboratory to the production scale thus poses numerous problems with respect to the reactant's mixing, temperature control (heat removal), catalyst selectivity and deactivation [5]. The performance of such processes can be predicted analytically to only a limited extent for reactors with well-defined flow patterns.

15.2
General Criteria for Reactor Choice and Design

Various parameters must be considered when selecting a reactor for multiphase reactions, such as the number of phases involved, the differences in the physical properties of the participating phases, the post-reaction separation, the inherent reaction nature (stoichiometry of reactants, intrinsic reaction rate, isothermal/adiabatic conditions, etc.), the residence time required and the mass and heat transfer characteristics of the reactor. For a given reaction system, the first four aspects are usually controlled to only a limited extent, if at all, while the remainder serve as design variables to optimize reactor performance. High rates of heat and mass transfer improve effective rates and selectivities and the elimination of transport resistances, in particular for the rapid catalytic reactions, enables the reaction to achieve its "chemical" potential in the optimal temperature and concentration window. Transport processes can be ameliorated by greater heat exchange or interfacial surface areas and short diffusion paths. These are easily attained in microstructured reactors.

The characteristic time of chemical reactions, t_r, which is defined by intrinsic reaction kinetics, can vary from hours (for slow organic or biological reactions) to milliseconds for high-temperature (partial) oxidation reactions (Figure 15.1). When the reaction is carried out in a reactor, heat and mass transfer interfere with the reaction kinetics.

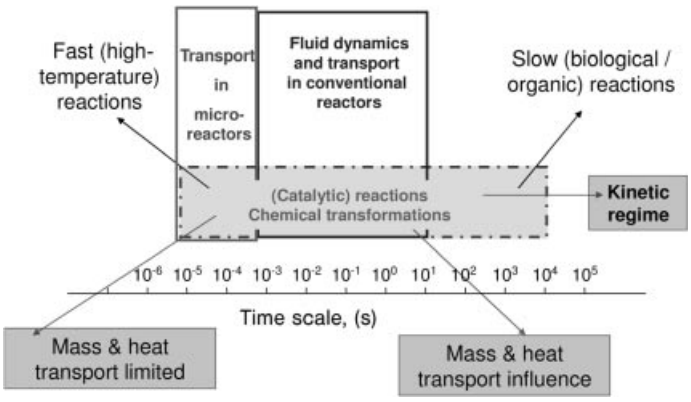

Figure 15.1 Time scale of chemical and physical processes.

The characteristic time of physical processes (heat/mass transfer) in conventional reactors ranges from 10 to 10^{-3} s. This means that relatively slow reactions ($t_r \gg 10$ s) are carried out in the kinetic regime and the global performance of the reactor is controlled by the intrinsic reaction kinetics. The chemical reactor is designed and dimensioned to achieve the required product yield and conversion of the raw material. The attainable reactant conversion in the kinetic regime depends on the ratio of the residence time in the reactor, τ, to the characteristic reaction time, t_r. This ratio is known as the first Damköhler number, *DaI*:

$$DaI = \frac{\tau}{t_r} \tag{15.1}$$

Depending on the kinetics and the type of the reactor, the residence time should be several times higher than the characteristic reaction time to obtain conversions >90% [6, 7].

For fast chemical reactions, the characteristic reaction time is of the same order of magnitude as the characteristic time of the physical processes (Figure 15.1). The performance of a conventional reactor is influenced in this case by mass and/or heat transfer. For very fast reactions, the global transformation rate may be completely limited by transfer phenomena. As a result, the reactor performance is diminished compared with the maximum performance attainable in the kinetic regime and the product yield is very often reduced.

To eliminate mass transfer resistances in practice, the characteristic transfer time should be roughly one order of magnitude smaller than the characteristic reaction time. As the mass and heat transfer performance in a microstructured reactor (MSR) is up to two orders of magnitude higher than in conventional tubular reactors, the reactor performance can be considerably increased, leading to the desired intensification of the process. In addition, consecutive reactions can be efficiently suppressed due to strict control of the residence time and a narrow residence time distribution (RTD). Therefore, fast reactions carried out in a MSR show higher product selectivity and yield.

Although microstructured reactors possess many advantages over conventional equipment, the following case-specific drawbacks should be envisaged in conventional processing options:

- severe transport limitations (heat or mass transfer)
- low yields and high wastage due to multistep reactions
- high dilutions with inerts or solvents for safety
- poor control of reaction parameters
- failure to meet market quality demand.

15.3 Fluid–Solid Reactors

Fluid–solid systems cover a major class of chemical reactions and encompass both liquid–solid and gas–solid systems. In either case, the fluid phase is a single homogeneous fluid. The solid phase acts as a catalyst and its arrangement in the

main reactions zone is an important and complex task. Two types of fluid–solid MSR have been described in the literature for different applications: the fixed-bed reactor and the catalytic wall reactor. Fixed-bed MSRs accommodate a large amount of catalyst as particles of size ~10–250 μm depending on the reactor diameter, offering a large geometric specific surface area for chemical reactions. The randomly micro-packed-bed reactor is mainly used for catalyst screening. The advantage of packed-bed MSRs stems from the fact that the developed catalyst used in traditional reactors can be applied. However, high pressure drops and fluid maldistribution due to irregular catalyst packing limit the performance of such reactors, especially at very low channel diameters.

The catalytic wall reactor with channel diameters in the range 50–1000 μm and a length dependent on the reaction time required circumvents these shortcomings. However, in most cases, the catalytic surface area provided by the wall alone is insufficient for the chemical transformation and therefore the specific surface area has to be increased by chemical treatment of channel walls or by coating them with highly porous support layers. This can be done by using a variety of techniques such as sol–gel, electrophoretic and chemical or physical vapor deposition [8, 9].

The three fundamental operational parameters described below characterize the MSR: pressure drop, residence time distribution and mass transfer rates.

15.3.1 Pressure Drop

The pressure drop during the passage of a fluid through a reactor is an important parameter related to the optimization of the energy consumption. Pressure drop will be considered assuming non-compressible fluids and taking the standard assumption of continuum mechanics. Gas properties at temperatures up to ~600 K and at a minimum pressure of 0.1 MPa will be used. Fluid velocities less than 10 m s^{-1} will be considered in channels with hydraulic diameters less than 1 mm. Under these conditions, the fluid flow is laminar and compressibility effects can be neglected [10].

To avoid flow maldistribution in the bed, the particle diameter should not be larger than one-tenth of the tube diameter ($d_p \leq d_t/10$) and the channel length should be higher than 50 particle diameters ($L_{bed} > 50 d_t$). This may lead to a relatively high pressure drop in the MSR, which can be estimated with the modified Ergun equation [11]:

$$\Delta p = 160 \frac{(1-\varepsilon)^2}{\varepsilon^3} \frac{\mu u}{d_p^2} + 3.1 \frac{(1-\varepsilon)}{\varepsilon^3} \frac{\rho u^2}{d_p} \left[\frac{\mu(1-\varepsilon)}{\rho u d_p} \right]^{0.1} L_{bed} \tag{15.2}$$

Therefore, microstructured multichannel reactors with catalytically active walls are by far the most often used devices for heterogeneous catalytic reactions. Advantages are low pressure drop, high external and internal mass transfer performance and a quasi-isothermal operation. In most cases the reactors are based on micro heat exchangers as shown in Figure 15.2. Typical channel diameters are in the range of

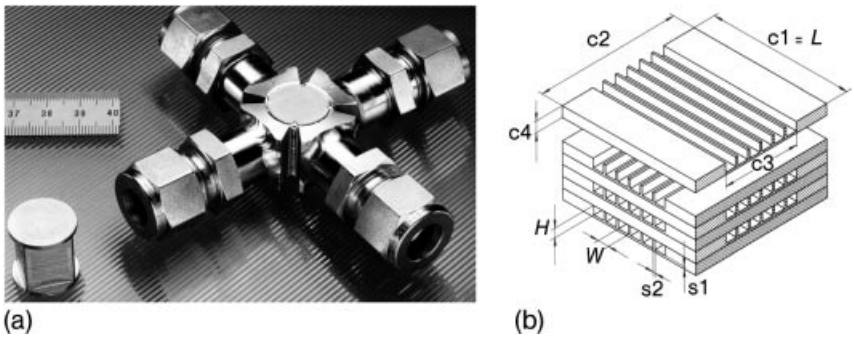

Figure 15.2 (a) Photograph and (b) schematic representation of a microstructured heat exchanger/reactor (Forschungszentrum Karlsruhe [1]). Channel length $L = 14$ mm, width $W = 100\,\mu$m, height $H = 78\,\mu$m.

50–500 μm with a length between 20 and 100 mm. About 200–2000 channels are assembled in one unit.

The pressure drop through open channels with laminar flow is given by the Hagen–Poiseuille equation [11]):

$$\Delta p = 32\zeta \frac{\mu u}{d_t^2} L_t \tag{15.3}$$

where ζ is a geometric factor, which is 1 for a circular tube, and depends on the height (H) to width (W) ratio for a rectangular channel. The correction factor becomes 0.89 for quadratic channels and assumes the asymptotic value 1.5 when the ratio goes to zero. An empirical correlation is given by the following expression [8]:

$$\zeta = 0.8735 + 0.6265 \exp\left(-3.636 \frac{H}{W}\right) \tag{15.4}$$

15.3.2
Residence Time Distribution

The residence time distribution (RTD) is a probability distribution function used to characterize the time of contact and contacting pattern (such as for plug-flow or complete backmixing) within the reactors. Excessive retention of some elements and shortcircuiting of others due to backmixing and other dispersive phenomena lead to a broad distribution in the residence times of individual molecules in the reactor. This tends to decrease conversion and exerts a negative influence on product selectivity/yield. The RTD depends on the flow regime and is characterized by Reynolds (Re) and Schmidt (Sc) numbers.

An idealized continuous flow MSR can be described by plug flow behavior, meaning that all molecules at the reactor outlet exhibit an identical residence time. Non-idealities in tubular reactors can be characterized using the axial dispersion

model, which assumes that the RTD may be considered as the result of ideal plug flow with superimposed longitudinal dispersion due to microconvective flows, but treated as diffusive mass transfer. For a constant effective dispersion coefficient D_{ax} (analogous to the molecular diffusion coefficient, D_m, but much greater), the mass flux given by Fick's law is

$$J = -D_{ax}\frac{\partial c}{\partial z} \tag{15.5}$$

Considering the mass flux entering and leaving an infinitesimally small element in a tubular reactor and integrating with the open boundary conditions, the response to a tracer pulse at the reactor inlet can be predicted at the reactor outlet from the following equation [6]):

$$C(\theta) = \frac{1}{2}\sqrt{\frac{Bo}{\pi\theta}}\exp\left[\frac{-(1-\theta)^2 Bo}{4\theta}\right] \tag{15.6}$$

where

$$C = \frac{c}{c_0}; \quad c_0 = \frac{n_{inj}}{V_R}; \quad \theta = \frac{t}{\tau}; \quad \tau = \frac{L_t}{u}; \quad Bo = \frac{uL}{D_{ax}}$$

The extremes of the reactor hydrodynamics can be characterized by the Bodenstein numbers:

$$Bo = {L_t}^2/D_{ax}\,\tau = t_{D_{ax}}/\tau \to 0 \quad \text{complete backmixing}$$

$$Bo = {L_t}^2/D_{ax}\tau = t_{D_{ax}}/\tau \to \infty \quad \text{no dispersion} \tag{15.7}$$

where $t_{D_{ax}}$ is the characteristic axial dispersion time. In practice, a plug-flow behavior is considered at $Bo \geq 100$).

Axial dispersion is also given by means of the Peclet number, which uses the tube diameter or particle diameter in a fixed bed as characteristic length. It is defined as

$$Pe = \frac{ud_t}{D_{ax}} = Bo\frac{d_t}{L_t} \tag{15.8}$$

Hence the axial dispersion is quantified by fitting the above equations to experimental tracer concentration–time profile. Some of the experimental techniques applied to characterize an MSR are listed in Table 15.2. The following points should be borne in mind in connection with the RTD for an MSR:

- For ease of interpretation, it is important that the input tracer signal should be an ideal Dirac delta function. This is difficult to achieve manually, especially when distortion by peripheral equipment is taken into consideration.
- MSRs are particularly sensitive to flow distortion as a result of tracer injection.
- In most conventional equipment, the value of *Re* is far higher than in an MSR and the operational regime is thus either transitional or turbulent.

Table 15.2 Various techniques used for RTD in MSRs.

Tracer	Characterization method	Type of MSR	Reference
Feed: nitrogen Tracer: argon or helium	Mass spectrometry	Stacked plate reactor	Rouge [12]
Feed: water Tracer: dye (Malachite Green oxalate)	Optical (transmittance sensor)	PTFE tube	Günther *et al.* [13]
Feed: ethanol Tracer: fluorescent – Rhodamine B	Fluorescence microscopy measurements	Rectangular microchannel	Trachsel *et al.* [14]
Feed: water Tracer: Basic Blue 3	Spectroscopic measurements	Micromixer	Boskovic and Loebbecke [15]

- Care should be taken that neither the tracer input junction (usually T-type) nor the bends in the MSR give rise to any dead volume
- Due to the large surface-to-volume ratio and no-slip boundary conditions, it may be that a large amount of tracer is retained at the reactor wall if the tracer has an affinity towards the solid material. In such cases, adhesion should be suppressed using a surfactant in the liquid.

Mears [16] proposed a criterion based on the conversion obtained for an irreversible reaction which deviates ~5% from the conversion under ideal plug-flow behavior to estimate the corresponding Bodenstein number:

$$Bo > \frac{20n}{\ln(1-X)} \tag{15.9}$$

where n is the reaction order.

Flow in microchannels with diameters between 10 and 500 μm is mostly laminar and has a parabolic velocity profile. Therefore, the molecular diffusion in the axial and radial directions plays an important role in the RTD. The diffusion in the radial direction tends to diminish the spreading effect of the parabolic velocity profile, whereas in the axial direction the molecular diffusion increases the dispersion. Taylor [17] and Aris [18] established the following relation to predict the effective axial dispersion coefficient:

$$D_{ax} = D_m + \chi \frac{u^2 d_t^2}{D_m} \tag{15.10}$$

with $\chi = 1/192$ for circular tubes.

The Bodenstein number in microchannels can be determined with

$$\frac{1}{Bo} = \frac{D_m}{{L_t}^2}\frac{L_t}{u} + \frac{1}{192}\frac{d_t^2}{D_m}\frac{u}{L_t} = \frac{D_m}{{L_t}^2}\frac{L_t}{u} + \frac{1}{192}\frac{4R_t^2}{D_m}\frac{u}{L_t},$$
$$\frac{1}{Bo} = \frac{\tau}{t_{D,ax}} + \frac{1}{48}\frac{t_{D,rad}}{\tau} \tag{15.11}$$

where

$$t_{D,ax} = \frac{L_t^2}{D_m};\quad t_{D,rad} = \frac{{R_t}^2}{D_m}$$

The first term in Equation (15.11) corresponds to the ratio between space time and the characteristic axial diffusion time. The molecular diffusion coefficient lies in the order of $10^{-5}\,m^2\,s^{-1}$ for gases and $10^{-9}\,m^2\,s^{-1}$ for liquids. Typical lengths of an MSR are several centimeters and the space time is in the range of seconds. Therefore, the axial dispersion in microchannels is mainly determined by the second term in Equation (15.11) and the Bodenstein number can be estimated with the equation

$$Bo \cong 48\frac{\tau}{t_{D,rad}} \cong 50\tau\frac{D_m}{{R_t}^2} \tag{15.12}$$

It follows that axial dispersion can be neglected ($Bo \geq 100$), if the space time is at least twice the radial diffusion time, $t_{D,rad}$. Accordingly, axial dispersion of gases in microchannels can be neglected if their diameters are less than 1000 µm and the space time is longer than 0.1 s. This has also been proved experimentally [19, 20].

Due to the small volume of a single channel, many channels have to be used in parallel to obtain sufficient reactor performance as shown in Figure 15.2. A uniform distribution of the reaction mixture over thousands of microchannels is necessary. Flow maldistribution will enlarge the RTD in the multitubular reactor and lead to a reduced reactor performance along with reduced product yield and selectivity [10, 19, 21]. Therefore, several authors have reported designs of flow distribution manifolds [10, 21, 22].

In addition to maldistribution, small deviations in the channel diameter introduced during the manufacturing process cause an enlargement of the RTD. The deviations may also be due to a non-uniform coating of the channel walls with catalyst layers. If the number of parallel channels is large ($N > 30$), a normal distribution of the channel diameters with a standard deviation σ can be assumed. The relative standard deviation, $\sigma_d^2 = \sigma_d/\bar{d}_t$ influences the pressure drop over the microreactor [23]:

$$\Delta p = \frac{128\mu Q_{tot} L}{\pi N \bar{d}_t^{\,4}\left(1 + 6\hat{\sigma}_d^{\,2}\right)} \tag{15.13}$$

Equation (15.13) shows that a variation of the channel diameter changes the pressure drop at a constant overall volumetric flow. As the pressure drop for each channel is identical, the variation of the diameter results in a variation of the individual flow rates, R_i and the residence time, $\tau_i = V_i/Q_i$.

Supposing there is plug flow in each channel ($Bo_i \rightarrow \infty$), the overall dispersion is inversely proportional to the relative standard deviation and can be estimated using the following equation [24]:

$$Bo_{reactor} \cong \frac{{d_t}^2}{2{\sigma_d}^2} \tag{15.14}$$

In consequence, the plug-flow behavior in a multichannel microreactor ($Bo_{reactor} \geq 100$) can only be assumed if the relative standard deviation is $\sigma_d/d_t \leq 0.07$.

15.3.3 Mass Transfer and Chemical Reaction

In fluid–solid systems, the reaction takes place on the catalyst surface. Prior to this, the reactant molecules have first to reach the catalyst surface and, therefore, the rate of mass transfer is an important operational parameter (Figure 15.3). Two types of mass transfer need to be considered in fluid–solid reactions: external and internal mass transfer. In particular, internal mass transfer limitations should be avoided, since they more often limit the performance of the reactor and more strongly influence the product selectivity. The internal mass transfer is characterized by an effectiveness factor, η, defined as the ratio of the observed reaction rate to that at constant concentration throughout the catalyst layer. To ensure an effectiveness factor of $\eta \geq 0.95$ in an isothermal catalyst layer, the following criterion must be fulfilled [16]:

$$\delta_{cat,max} \leq b\sqrt{\frac{D_{eff}\, c_s}{r_{eff}}} \tag{15.15}$$

where D_{eff} and r_{eff} are the effective diffusion coefficient and the observed reaction rate, respectively. The coefficient b depends on the formal reaction order and has a value of 0.8, 0.3 and 0.18 for zero-, first- and second- order reactions, respectively.

In the case of strongly exothermic and endothermic reactions, the reactions may give rise to a temperature profile within the catalytic layer, which is dependent on reaction enthalpy (ΔH_R), activation energy (E) and the thermal conductivity of the porous catalytic material (λ_{eff}). For quasi-isothermal behavior, the observed rate, r_{eff},

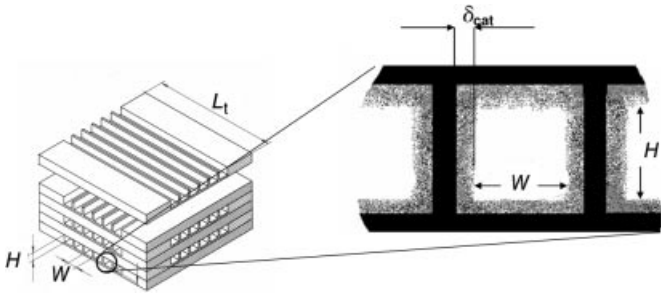

Figure 15.3 Mass transfer and heterogeneous catalytic reaction in wall reactors.

should not differ from the rate that would be observed at constant temperature by more than 5% and therefore the resulting criterion for effectively isothermal catalytic wall behavior is given by

$$\delta_{\text{cat,max}} \leq 0.3\sqrt{\frac{R}{E}\frac{\lambda_{\text{eff}}\,{T_s}^2}{|\Delta H_R| r_{\text{eff}}}} \tag{15.16}$$

where T_s is the temperature of the catalyst surface and R is the gas constant.

In general, the thickness of the catalytic layer is kept sufficiently small to avoid the influence of internal mass transfer on the kinetics. In this way, only the transfer of the reactants from the bulk to the catalytic wall must be considered and the reaction rate per unit outer surface area of the catalytic layer. For an irreversible first-order reaction, the rate is given by

$$r_s = k_s c_{1,s} \tag{15.17}$$

The molar flux from the fluid phase to the surface of the layer is proportional to the concentration gradient between the bulk and the surface:

$$J_1 = k_G(c_{1,b} - c_{1,s}) \tag{15.18}$$

Under stationary conditions, the molar flux from the fluid phase reaching the catalytic surface and the rate of transformation per surface unit must be identical: $J_1 = r_s$. It follows that for a first-order reaction

$$k_s c_{1,s} = k_G(c_{1,b} - c_{1,s}) \tag{15.19}$$

Solving Equation (15.19) for the concentration of A_1 at the catalyst surface gives

$$c_{1,s} = \frac{k_G}{k_G + k_s} c_{1,b} = \frac{1}{1 + DaII} c_{1,b} \tag{15.20}$$

and for the observed (effective) reaction rate

$$r_{s,\text{eff}} = k_s \frac{k_G}{k_G + k_s} c_{1,b} = k_s \frac{1}{1 + DaII} c_{1,b} \tag{15.21}$$

The effective reaction rate is determined by the ratio of the characteristic mass transfer time, t_D, and the characteristic reaction time, t_r, the second Damköhler number:

$$DaII = \frac{t_D}{t_r} = \frac{k_s}{k_G} \tag{15.22}$$

Low values of $DaII$ ($t_D \ll t_r$) correspond to a situation where the effect of the mass transfer can be neglected. The observed reaction rate is close to the intrinsic rate:

$$r_{s,\text{eff}} = k_s \frac{1}{1 + DaII} c_{1,b} \cong k_s c_{1,b} = r_s \tag{15.23}$$

At high values of $DaII$, the rate of the transformation is completely limited by mass transfer from the fluid phase to the surface, the surface concentration being

nearly zero ($c_{1,s} \cong 0$):

$$r_{s,eff} = k_s \frac{1}{1 + DaII} c_{1,b} \cong k_G c_{1,b} = J_1 \tag{15.24}$$

The existence of a significant difference between the concentration in the bulk of the fluid phase and the surface of the catalytic layer leads to lower reaction rates for positive reaction orders. This can be expressed by the external effectiveness factor η_{ex}:

$$\eta_{ex} = \frac{r_s(c_{1,s})}{r_s(c_{1,b})} = \frac{r_{s,eff}}{r_s(c_{1,b})} \tag{15.25}$$

For an intrinsic first-order reaction, Equation (15.25) becomes

$$\eta_{ex} = \frac{1}{1 + DaII} \tag{15.26}$$

Due to the small channel diameters in MSRs, laminar flow can be considered. The radial velocity profile in a single channel develops from the entrance to the position where a complete Poiseuille profile is established. The length of the entrance zone depends on the Reynolds number and can be estimated from the following empirical relation [25, 26]:

$$L_e \leq 0.06 \; Re \, d_t \tag{15.27}$$

Within the entrance zone, the mass transfer coefficient diminishes, reaching a constant value. The dependency can be described with Equation (15.28) in terms of the Sherwood number, $Sh = k_G d_t / D_m$ [27, 28]:

$$Sh = B\left(1 + 0.095 \frac{d_t}{L} ReSc\right)^{0.45} \tag{15.28}$$

where the constant B corresponds to the asymptotic Sherwood number for constant concentration at the wall, which is identical with the asymptotic Nusselt number Nu, characterizing the heat transfer in laminar flow at constant wall temperature. The constant B depends on the geometry of the channel as summarized in Table 15.3.

Table 15.3 Mass transfer characteristics for different channel geometries [27].

Geometry	B
Circular	3.66
Ellipse (width/height = 2)	3.74
Parallel plates	7.54
Rectangle (width/height = 4)	4.44
Rectangle (width/height = 2)	3.39
Square	2.98
Equilateral triangle	2.47
Sinusoidal	2.47
Hexagonal	3.66

If the entrance zone in the tube can be neglected, the mass transfer is constant and given by B. It follows for a circular-shaped reactor:

$$Sh_\infty = 3.66; \text{ for } L \geq 0.05 ReScd_t \quad \text{(constant wall concentration)} \tag{15.29}$$

If the mass transfer is accompanied by a chemical reaction at the catalyst surface on the reactor wall, the mass transfer depends on the reaction kinetics [29]. For a zero-order reaction the rate is independent of the concentration and the mass flow from the bulk to the wall is constant, whereas the reactant concentration at the catalytic wall varies along the reactor length. For this situation the asymptotic Sherwood number in circular tube reactors becomes $Sh'_\infty = 4.36$ [29]. The same value is obtained when reaction rates are low compared with the rate of mass transfer. If the reaction rate is high (very fast reactions), the concentration at the reactor wall can be approximated to zero within the whole reactor and the final value for Sh is $Sh_\infty = 3.66$. As a consequence, the Sherwood number in the reaction system depends on the ratio of the reaction rate to the rate of mass transfer characterized by the second Damköhler number defined in Equation (15.22).

Villermaux [29] proposed a simple relation to estimate the asymptotic Sherwood number as function of $DaII$:

$$\frac{1}{Sh''_\infty} = \frac{1}{Sh'_\infty} + \frac{DaII}{DaII + 1.979}\left(\frac{1}{Sh_\infty} - \frac{1}{Sh'_\infty}\right) \tag{15.30}$$

Hence the mass transfer coefficient in multi tubular MSR depends on, in addition to the molecular diffusion coefficient, the channel diameter d_t and the second Damköhler number $DaII$:

$$k_G = \frac{Sh''_\infty D_m}{d_t} \tag{15.31}$$

The specific performance of the MSR under mass transfer limitations depends on the mass transfer coefficient and the specific surface area of the channel, a:

$$a = \frac{4}{d_t} \text{circle}; \quad a = \frac{2(W+H)}{WH} \text{rectangle} \tag{15.32}$$

The product $k_G a$ is called volumetric mass transfer coefficient, which determines the maximum reactor performance for very fast catalytic reactions. Its value increases with $1/d_t^2$ for circular and with $1/d_h^2$ for rectangular channels. This is shown for different channel geometries in Figure 15.4.

15.4 Fluid–Fluid Reactors

15.4.1 Gas–Liquid Systems

Gas–liquid contactors exist in a number of configurations. Mass transfer can take place from the gas phase to the liquid phase as well as in the reverse direction.

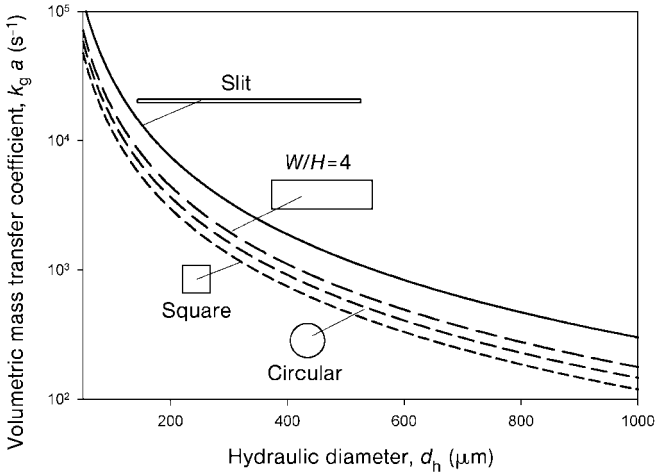

Figure 15.4 Volumetric mass transfer coefficient as a function of the hydraulic diameter in microstructured channels ($D_m = 10^{-5}\ m^2\ s^{-1}$).

Chemical reactions may occur in the gas and/or in the liquid phase, respectively. In gas–liquid MSRs, different mixing patterns such as plug flow, well-mixed or plug flow with axial dispersion are observed. Above all, plug flow (referred to as slug, Taylor or bubble train flow) is one of the most stable flow regimes observed in microchannels and provides a high specific interfacial area for mass transfer. Industrially important examples of gas–liquid mass transfer followed by chemical reactions in the liquid phase include gas purification, oxidation, chlorination, hydrogenation and hydroformylation processes.

Especially relatively fast reactions benefit from the excellent mass transfer characteristics of the MSR. Additionally, exothermic reactions also benefit due to the superior removal of heat produced during the reaction. The examples of different gas–liquid reactions which have already been studied in MSRs are listed in Table 15.4.

Mass transfer with simultaneous chemical reaction is characterized using the reaction–diffusion modulus known as the Hatta number, defined as the ratio of the reaction in the film to the mass transfer rate through it. Thus, for a first-order reaction the Hatta number is given by

$$Ha = \frac{\sqrt{k_r D_m}}{k_L} \tag{15.33}$$

If Ha is >3, then the reactions are considered fast and proceed mainly within the liquid film near the gas–liquid interface, whereas if Ha is <0.3, the reactions are slow and occur mainly in the bulk liquid.

In gas–liquid MSRs, the characteristic dimensions of the liquid phase differ from those of the bulk phase in conventional reactors. Frequently, the mass transfer models used for MSR assume a finite depth of the liquid phase. In this context, two additional dimensionless parameters are introduced: the degree of saturation and the

Table 15.4 Examples of gas–liquid reactions carried out in MSRs.

Reaction	Reactor	Reference
Direct fluorination of toluene and nitrotoluene	Falling film and bubble column MSR	Jähnisch *et al.* [30]
Selective fluorination of 4-nitrotoluene, 1,3-dicarbonyl and heterocyclic compounds	Single-channel MSR operating in annular flow regime	Chambers *et al.* [31]
Chlorination of acetic acid	Falling film MSR	Wehle *et al.* [32]
Photochlorination of toluene-2, 4-diisocyanate (TDI)	Falling film MSR	Ehrich *et al.* [33]
Nitration of naphthalene using N_2O_5	Interdigital mixers and MSR with the split–recombine technique	Antes *et al.* [34]
Oxidation of alcohols and Baeyer–Villiger oxidation of ketones using elemental fluorine	Single-channel MSR operating in annular flow regime	Chambers *et al.* [35]
Sulfonation of toluene with gaseous sulfur trioxide	Falling film MSR	Müller *et al.* [36]
Asymmetric hydrogenation of (*Z*)-methyl acetamidocinnamate with rhodium chiral diphosphine complexes	Mesh MSR	Abdallah *et al.* [37]

degree of utilization of the bulk liquid. The degree of saturation of the bulk liquid is the ratio of the liquid phase concentration of a solute to that at saturation. For an increasing reaction rate or a decreasing mass transfer rate, the degree of saturation will be low, approaching zero, and for a decreasing reaction rate or an increasing mass transfer rate, the degree of saturation will approach unity.

The degree of utilization of the liquid phase is the ratio of the actual transformation rate of a solute to that which would occur if the entire bulk phase was in equilibrium with the gas phase. For an increasing reaction rate or a decreasing mass transfer rate, the degree of utilization will diminish and finally approach zero.

The film model according to the Hinterland concept assumes a stagnant film independent of the liquid bulk [38]. The penetration model [39] assumes that elements of liquid film are mixed up with the liquid bulk after a certain superficial exposure time. Therefore, all the species present inside the liquid film are considered to be part of the liquid phase. This results in a larger overall liquid phase concentration. For processes controlled by intrinsic reaction kinetics ($Ha < 0.3$), the two approaches yield similar results, because most species are present in the bulk liquid and the excess of species present in the liquid film can be neglected. For processes controlled completely or partly by the rate of the mass transfer ($Ha > 0.3$), the two models give different results, because the excess of species present in the liquid film can no longer be neglected when compared with the total amount of species present in the liquid phase (see Chapter 11).

15.4.1.1 Pressure Drop

The two fundamental flow patterns formed in gas–liquid MSR are the Taylor (slug or bubble) flow and the parallel (segregated) flow (Figure 15.5). Two models have been proposed [40]: (1) the homogeneous model, with mean flow velocity similar to single-phase flow, and (2) the separated flow model, with an artificially separated gas and liquid flow.

One of the most commonly used models to characterize the pressure drop in MSR is that proposed by Lockhart and Martinelli [41] for *gas–liquid horizontal flow* in pipes, which is used for all regimes. It employs two friction multipliers for gas and liquid, $\Phi_G{}^2$ and $\Phi_L{}^2$, as given by the following equation:

$$\left(\frac{\Delta p_f}{\Delta z}\right)_{2p} = \Phi_G{}^2 \left(\frac{\Delta p_f}{\Delta z}\right)_G \text{ or } \left(\frac{\Delta p_f}{\Delta z}\right)_{2p} = \Phi_L{}^2 \left(\frac{\Delta p_f}{\Delta z}\right)_L \tag{15.34}$$

These equations are correlated in terms of a dimensionless number called the Lockhart–Martinelli parameter (ψ), which is the ratio of the single-phase pressure drop of liquid to that of the gas and is given by

$$\psi = \frac{\left(\frac{\Delta p_f}{\Delta z}\right)_L}{\left(\frac{\Delta p_f}{\Delta z}\right)_G} \tag{15.35}$$

The relationship between $\Phi_L{}^2$ and ψ can be obtained from the widely-used Chisholm's equation [42]:

$$\Phi_L{}^2 = 1 + \frac{C}{\psi} + \frac{1}{\psi^2} \tag{15.36}$$

where C is a constant, ranging from 5 to 20 depending on the flow pattern of gas and liquid in the channel. In the case of MSR, the Reynolds number for both the liquid and gas phases are less than 1000 and the constant C is considered to be 5 [42].

However, from experimental measurements, Yue *et al.* [43] reported for the CO_2–water system that the friction multiplier cannot be predicted reliably with a

Figure 15.5 Taylor and annular flow in vertical capillary. Adapted from Liu *et al.* [45].

single value of C. It was found to become greater with increasing mass flux and, therefore, a new correlation was proposed with a standard deviation of 9.2%:

$$C = 0.185\psi^{-0.0942} Re^{0.711} \tag{15.37}$$

This equation shows that the Lockhart–Martinelli method is still applicable for representing the two-phase frictional pressure drop in the microchannel if the appropriate C value is employed. Even so, it is not recommended to extrapolate the Lockhart–Martinelli correlations down to very small channels due to the absence of surface tension forces considered in the model. Besides, the model does not account for the two-phase flow patterns. Chen *et al.* [44] collected 11 sets of literature data for two-phase pressure drops in small diameter tubes and found that neither the Lockhart–Martinelli correlations nor the homogeneous models accurately follows the experimental data. Therefore, they modified the homogeneous model including a Bond [body (gravitational) forces/surface tension forces] and a Weber number (inertial force/surface tension force) together with other related dimensionless groups suggesting a general model for practical applications.

Liu *et al.* [45] developed a flow regime-dependent relationship for estimating the total pressure drop in two-phase *vertical capillary flows*. They considered a single-phase vertical tube with liquid flowing in the laminar regime. The total pressure drop (Δp_{tot}) is composed of two contributions: (1) the pressure drop due to frictional effects of the liquid flow (Δp_f) and (2) the hydrostatic pressure of the liquid:

$$\Delta p_{tot} = \Delta p_f + \rho_L g L_t \tag{15.38}$$

For laminar flow, the frictional pressure drop is given by the Hagen–Poiseuille equation

$$\Delta p_f = \frac{32\mu_L u_L L_t}{{d_t}^2} \tag{15.39}$$

Combining both equations, the total pressure drop is given by

$$\Delta p_{tot} = \frac{32\mu_L L_t}{{d_t}^2}\left[u_L + \left(\frac{{d_t}^2}{32\mu_L}\right)\rho_L g\right] \tag{15.40}$$

By comparing Equations (15.39) and (15.40), a gravity equivalent liquid velocity (u_e) in the capillary can be introduced that would result in a pressure loss equal to the hydrostatic pressure exerted by the liquid phase. Assuming laminar flow, the gravity equivalent liquid velocity becomes

$$u_e = \left(\frac{{d_t}^2}{32\mu_L}\right)\varepsilon_L \rho_L g \tag{15.41}$$

The two-phase mixture velocity u_E is defined as the sum of the superficial velocities of the two phases and the gravity equivalent velocity (u_e):

$$u_E = u_G + u_L + u_e \tag{15.42}$$

A dimensionless two-phase pressure factor f_E can be defined, analogous to the Fanning friction factor [46]:

$$f_E = \frac{\Delta p_{tot}/L_t}{1/2\rho_L u_E^2(4/d_t)} \tag{15.43}$$

In a situation where both the gas- and liquid-phase flows are laminar, the pressure factor can be expected to be, similarly to the Fanning friction factor

$$f_E = \frac{C}{Re_E} \tag{15.44}$$

with

$$Re_E = \frac{\rho_L u_E d_t}{\mu_L}$$

The constant C depends on the channel geometry and has values of 16 and 14.2 for circular and square channels, respectively.

For $u_G/(u_G + u_L) < 0.5$, homogeneous flow of the two-phase mixture can be assumed and the pressure factor can be estimated with Equation (15.44). At $u_G/(u_G + u_L) > 0.5$, a heterogeneous flow regime develops and a slip (s) between the two phases occurs, which can be calculated by

$$s = \frac{u_G/\varepsilon_G}{u_L/(1-\varepsilon_G)} \tag{15.45}$$

To predict the pressure drop for the heterogeneous flow regime as in Taylor flow, an empirical correlation for the friction factor was obtained from experimental data:

$$f_E = \frac{C}{Re_E} s^{-0.5}\left[\exp(-0.02 Re_E) + 0.07\ Re_E^{0.34}\right] \tag{15.46}$$

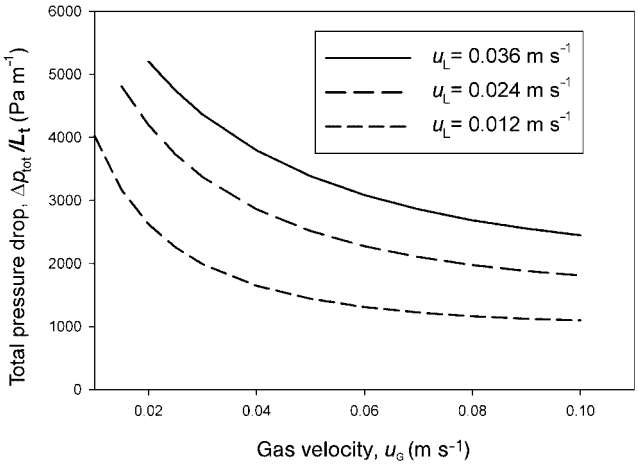

Figure 15.6 Pressure drop in upward gas–liquid flow in a square capillary. Air–water system, $d_t = 2$ mm.

for the velocity range $0.008 < (u_G + u_L) < 1\,m\,s^{-1}$). Figure 15.6 depicts the pressure drop for three liquid velocities in a square microchannel (upward air-water flow, $0.01 < u_G < 0.1$). Taylor flows occurs at such low flow rates and the Lockhart- Martinelli as well as the homogeneous model fails to predict the pressure drop.

15.4.1.2 Residence Time Distribution

As the reactor performance depends strongly on the residence time distribution, its prediction as function of the operational parameters is important.

For Taylor flow in a single channel, the degree of backmixing in the gas phase is less than that for homogeneous laminar flow. This is due to the presence of bubbles, which effectively seal packets of the liquid [47]. Mass transfer from one liquid slug to another thus takes place by diffusion from the slug to the wall film and subsequently from the film to another slug. However, if the orientation of capillary is changed from horizontal to vertical, the stagnant film becomes a falling film for upward flow [48], especially for square capillaries.

Analytical Model Thulasidas *et al*. [49] developed an analytical model for dispersion in a vertical capillary for gas–liquid flow by taking into account the gravity-driven flow in the film (Figure 15.7) and were able to predict experimental results. Mass transfer occurs at the surface between the liquid film and the vortex moving along the dividing streamline. The following assumptions were made:

- The velocity gradient in both the liquid slug and the wall film is negligible (i.e. plug flow).
- Bubbles and slugs have the same length.

As can be seen from the Figure 15.7, for a coordinate system moving with the bubble, the liquid film "flowing" at the side of the bubble comes in contact with the downward moving part of the vortex at the top of the slug. There is no convective mixing between these two regions while they traverse the length of the slug exchanging mass by diffusion only. At the bottom of the slug, the liquid film flows into the space between the capillary and the next bubble, while the vortex turns around and moves upwards. During the upward movement, the inner section of the vortex is isolated from the liquid film by the outside section and no appreciable mass

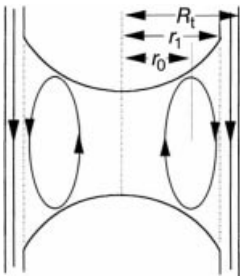

Figure 15.7 Schematic representation of the position of stagnant zone and dividing streamline. Adapted from Thulasidas *et al*. [49].

transfer takes place. After completing one circulation, the vortex again comes into contact with a liquid film of different concentration and the process is repeated until the slug leaves the capillary. According to this model, mass transfer processes occur in cycles, with the characteristic cycle time being that required for the vortex to complete one recirculation. During the cycle, the vortex exchanges mass with a liquid film of approximately twice the vortex length.

At the beginning of a cycle, the concentration of a given tracer chemical inside the recirculating region and the liquid film region are c_{10} and c_{20}, respectively. For a coordinate system moving with the bubble, the diffusion front moves down from top to bottom of the liquid slug at a constant velocity along the dividing streamline as represented by the following unsteady-state diffusion equation:

$$\frac{\partial c}{\partial t} = \frac{D_{\mathrm{m}}}{r}\left[\frac{\partial}{\partial r}\left(r\frac{\partial c}{\partial r}\right)\right] \tag{15.47}$$

Initial conditions are as follows:

$$\begin{aligned} &IC1 : c(t,r) = c_{10} - c^{+} \text{ for } 0 \le r \le r_1 \text{ at } t = 0 \\ &IC2 : c(t,r) = c_{20} - c^{+} \text{ for } r_1 \le r \le R \text{ at } t = 0 \end{aligned} \tag{15.48}$$

The boundary conditions are

$$\begin{aligned} &BC1 : \frac{\partial c}{\partial r} = 0 \text{ at } r = 0 \\ &BC2 : \frac{\partial c}{\partial r} = 0 \text{ at } r = R_{\mathrm{t}} \end{aligned} \tag{15.49}$$

The normalized concentration c^{+}, defined as an area-weighted average of the initial concentrations, is given by

$$c^{+} = \frac{c_{10}{r_1}^2 + c_{20}\left({R_{\mathrm{t}}}^2 - {r_1}^2\right)}{{R_{\mathrm{t}}}^2} \tag{15.50}$$

A general solution of Equation (15.48) is obtained by the separation of variables:

$$c(t,r) = \mathrm{e}^{-\lambda^2 D_{\mathrm{m}} t}\left[aJ_0(\lambda r) + bY_0(\lambda r)\right] \tag{15.51}$$

where J_0 and Y_0 are the Bessel functions of the first and second kind of order zero, respectively. Introducing the boundary conditions, the following equations are obtained for the tracer concentration in a plane normal to the capillary axis, the area-averaged concentrations for vortex region and the area-averaged concentration in the liquid film:

$$c(t,r) = c^{+} + \sum_{n=0}^{n\to\infty} \frac{2\mathrm{e}^{-{\lambda_n}^2 D_{\mathrm{m}} t} r_1 (c_{10} - c_{20}) J_1(\lambda_n r_1) J_0(\lambda_n r)}{{J_0}^2(Z_{\mathrm{on}}) Z_{\mathrm{on}} R_{\mathrm{t}}} \tag{15.52}$$

$$c_{\mathrm{avg}} = c^{+} + \sum_{n=0}^{n\to\infty} \frac{\mathrm{e}^{-{\lambda_n}^2 D_{\mathrm{m}} t} r_1^2 \times 4(c_{10} - c_{20}) J_1(\lambda_n r_1)\left[J_1(\lambda_n r_1) - (r_0/r_1) J_1(\lambda_n r_0)\right]}{{J_0}^2(Z_{\mathrm{on}}) {Z_{\mathrm{on}}}^2 ({r_1}^2 - {r_0}^2)} \tag{15.53}$$

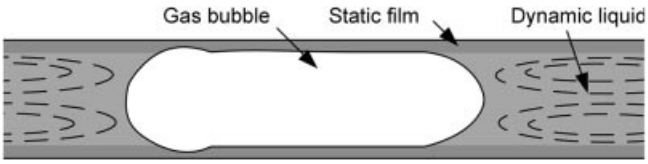

Figure 15.8 Schematics of gas–liquid (Taylor) flow in an MSR.

$$c_{\text{avg}} = c^{+} + \sum_{n=0}^{n\to\infty} \frac{e^{-\lambda_n^2 D_m t} r_1^{\,2} \times 4(c_{10} - c_{20}) J_1^{\,2}(\lambda_n r_1)}{J_0^{\,2}(Z_{\text{on}}) Z_{\text{on}}^{\,2}\left(R_t^{\,2} - r_0^{\,2}\right)} \tag{15.54}$$

where Z_{on} are the zeroes of the Bessel function of the first kind and order one.

The area-averaged concentration of the liquid film is used as the initial condition (c_{10}) for the following liquid slug and the area-averaged liquid film region concentration is ascertained by integration between the dividing streamline and the capillary wall. The position of the dividing streamline is given by [50]

$$\frac{r_1}{R_t} = 1 - \left(\frac{1.334 Ca^{\frac{2}{3}}}{1 + 3.334 Ca^{\frac{2}{3}}} \right) \tag{15.55}$$

The above equations can be used for square capillaries by mapping the square geometry into cylindrical coordinates and adjusting the contacting areas using geometric factors.

Continuum Model Kreutzer [47] used a continuum model to describe the RTD in Taylor flow by considering two zones (piston exchange model): a stagnant liquid film neglecting gravity and liquid slugs in plug flow (Figure 15.8). In this instance, the tracer concentrations in the recirculating region and the film region are referred to as c_{dyn} and c_{st}, respectively. The partial differential equations can be written as

$$\begin{aligned} &\text{Liquid slug}: \ \frac{\partial c_{\text{dyn}}}{\partial t} = -u_{\text{dyn}} \frac{\partial c_{\text{dyn}}}{\partial z} - \frac{k_{\text{SF}} a}{\phi} \left(c_{\text{dyn}} - c_{\text{st}} \right) \\ &\text{Wall film}: \ \frac{\partial c_{\text{st}}}{\partial t} = \frac{k_{\text{SF}} a}{1 - \phi} \left(c_{\text{dyn}} - c_{\text{st}} \right) \end{aligned} \tag{15.56}$$

where ϕ is the fraction of liquid in the dynamic phase and $k_{\text{SF}}a$ is the mass transfer group expressed per unit channel volume. The higher the mass transfer group, the smaller is the amount of tracer that passes through the channel without exchanging with film. The last term on the right-hand side of the liquid slug equation and the right-hand side of wall film equation corresponds to the mass transfer between liquid slug and stagnant film. Therefore, the interfacial area, a, corresponds to the area between film and liquid slug.

At the moment of introduction of tracer into the tube, the tracer concentration in the film is in equilibrium with the tracer concentration in the slug, hence the initial condition for RTD experiments is different from that of the reacting mass transfer experiments. The high Sherwood number for the inlet transition region of the

channel is therefore not likely to represent the behavior of tracer experiments. The mass transfer parameter $k_{SF}a$ is given in terms of Sh by

$$k_{SF}a = \frac{Sh D_m}{d_t}\frac{4\varepsilon_L}{d_t} \tag{15.57}$$

The tracer response E-curve is calculated by numerically integrating Equation (15.56) and using the concentration–time curve at the inlet. The amount of tracer that does not exchange with the film shows up in the E-curve as a sharp peak, where the width of the peak is only determined by the tracer injection curve. The amount of tracer that is transferred to the film is slowly released to subsequent slugs and appears in the E-curve as a long tail.

Total Liquid Hold-up Assuming a similar film thickness for bubble and slug and ignoring the velocity of the film, the length fraction of slugs can be equated to the flow rate fraction by

$$\frac{L_s}{L_s + L_b} \approx \varepsilon_L \tag{15.58}$$

where ε_L is the dynamic hold-up of liquid in the capillary.

Thulasidas *et al.* [48] proposed a correlation to calculate the total liquid hold-up in the capillary:

$$\begin{aligned}\varepsilon_L &= 1-\varepsilon_G \\ &= 1-\frac{A_b}{A}+\frac{Q_f}{A v_b}\end{aligned} \tag{15.59}$$

where Q_f is the film flow in the capillary, given by

$$Q_f = \frac{\pi \rho g {R_t}^4}{8\mu}\left\{1+4\left(\frac{R_b}{R_t}\right)^4\left[\frac{3}{4}-\ln\left(\frac{R_b}{R_t}\right)-\left(\frac{R_b}{R_t}\right)^{-2}\right]\right\} \tag{15.60}$$

15.4.1.3 Mass Transfer and Film Saturation

Different approaches have been used to model the mass transfer performance of gas–liquid contactors. They comprise two main parts: the micro-model, describing the mass transfer between the gas and the liquid phase, and the macro-model, describing the mixing pattern within the individual gas and liquid phases. The micro-models assume two types of interfacial behavior: stagnant films and dynamic absorption in small elements at the contact surface. The most widely used micro-models are the stagnant film model and the penetration and surface renewal models. In the stagnant film model, it is postulated that mass transfer proceeds via steady-state molecular diffusion in a hypothetical stagnant film at the phase interface [51]. In the penetration model, the uniform residence time of a fluid element at the phase interface is the characteristic parameter [52], whereas in the surface renewal model, a constant probability of element replacement is assumed [53]. A combined approach, the film-penetration model, is also used, yielding a two-parameter model combining the stagnant film and penetration models [54, 55]. The application of suitable models to

various systems must be determined on a case-by-case basis. For dynamic systems, the penetration model is physically more realistic than the stagnant film model.

For the mass transfer contribution in the Taylor flow regime, the film thickness is of particular importance and many studies have been concerned with its characterization (see Chapter 11).

Gas–liquid mass transfer for the absorption of methane in water was studied by Bercic and Pintar [56] using different capillaries of diameter 1.5, 2.5 and 3.1 mm, and the following correlation for the estimation of the mass transfer coefficient, $k_L a$, was proposed:

$$k_L a = \frac{0.111(u_L + u_G)^{1.19}}{[(1-\varepsilon_G)L_{UC}]^{0.57}} \tag{15.61}$$

where L_{UC} is the unit cell length (i.e. the length of a pair of gas bubble and liquid slug). As can be seen from the above equation, the mass transfer coefficient can be considered to be independent of the capillary diameter.

Van Baten and Krishna [57] developed a model for rising Taylor bubble flow in circular capillaries by considering two contributions to mass transfer: (1) the caps (assumed to be hemispherical) at either end of the bubble and (2) the liquid film surrounding the bubble. They put forward the following relationship for the overall volumetric mass transfer coefficient (see Chapter 11):

$$k_L a = k_{L,cap} a_{cap} + k_{L,film} a_{film} \tag{15.62}$$

Their model provided excellent agreement with CFD simulation results for capillaries with diameters 1.5, 2 and 3 mm.

Vandu *et al.* [58] adopted a simplified approach to take the film contribution into account:

$$k_L a = C_1 \sqrt{\frac{D_m u_G}{L_{UC}}} \frac{1}{d_t} \tag{15.63}$$

A plot of experimental $k_L a$ values versus $\sqrt{D_m u_G / L_{UC}}/d_t$ shows a straight line for constant $C_1 = 4.5$, which is almost the theoretical value from the model for the film contribution. The agreement between the model and the experiment is reasonably good for both circular and square capillaries. Thus the model shows a dependence of $k_L a$ on capillary diameter. Furthermore, Vandu *et al.* [58] validated the applicability of the correlation and it was proposed that the relation performs well for $\sqrt{(u_G + u_L)/L_S} > 3$, which corresponds to a short film contact time and a dominant film contribution. Below this range, the film contribution to mass transfer diminishes as the liquid in the film begins to approach saturation.

In Taylor flow regimes, the liquid usually exhibits good wettability for the channel wall, forming a thin wall film over which the gas bubbles glide. The wall film provides a lubricating action to the enclosed bubbles, and, as a consequence, bubbles flow at relatively higher velocity than the liquid. The interfacial gas–liquid area is thus comprised of two parts: the lateral part (that of the wall film) and the perpendicular part (between the bubble and the adjacent liquid plug). Often the length of the bubble is many times greater than the channel diameter, so that the lateral part of the

interfacial area is many times greater than the perpendicular contribution. The thin liquid wall film becomes saturated with the absorbed component or exhausted of the liquid-phase reactant. In such cases, the lateral part of the interfacial area will become inactive and therefore it is important for the design of an MSR to determine conditions under which this part of interface remains active.

Pohorecki [59] investigated the effectiveness of the interfacial area for mass transfer in two-phase flow in an MSR. He developed criteria to avoid saturation of the liquid wall film in the case of physical absorption or liquid of the film for absorption with instantaneous chemical reaction:

$$\frac{L_b D_m}{\nu_b \delta_{film}^{\ 2}} \ll 1 \tag{15.64}$$

where D_m corresponds to the molecular diffusion coefficient of the reactant in the liquid phase. The above equation shows that reagent exhaustion in the liquid film can be avoided by decreasing the length of the bubble or by increasing the flow velocity.

15.4.2 Liquid–Liquid Systems

Various types of microstructured reactors/extractors have been developed and evaluated both in the laboratory and in industrial practice (see Chapter 8). As with gas–liquid systems, distinctive flow patterns have been observed for liquid–liquid systems in microchannel reactors. Parallel or stratified flow and slug flow (or plug flow, segmented flow, liquid train flow) are the two most stable flow patterns found (Figure 15.9). Slug flow comprises a series of alternating slugs (plugs) of one phase separated by the other. The mechanism of slug flow formation in terms of viscous and capillary forces was explained in detail by Tice *et al.* [60]. Each slug serves as an individual processing subvolume, which is highly uniform and guarantees well-defined interfacial area for mass transfer processes. A key feature of this type of MSR is the ability to manipulate the two transport mechanisms: convection within the individual slug and interfacial diffusion between adjacent slugs of different phases. More attention has been paid to slug flow due to following benefits over parallel flow:

- Solute is transferred both by convection within the slugs and by diffusion between two adjacent slugs, whereas the solute transfer in parallel flow is only diffusive.

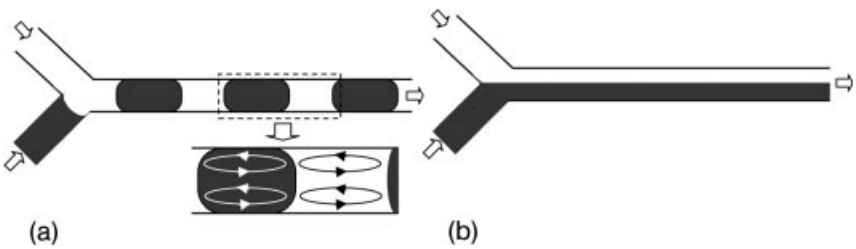

Figure 15.9 Stable flow patterns that can be achieved in the liquid–liquid flow capillary microreactor.

- It provides a significantly higher interfacial area than parallel flow in the presence of a wall film.
- It requires shorter processing times for the same throughput than parallel flow.
- Slug flow is highly stable over a wide operating window.
- In a given MSR length, the interfacial area can be controlled under a slug flow regime: increases in flow velocity decrease the slug size and thus provide a larger interfacial area. This variable is not possible for parallel flow. In addition, in the slug flow regime the increased flow rates intensify internal circulations within the slugs, which renew the interfacial surfaces with higher frequency, thus enhancing the diffusive penetration.

Apart from microchannels, dispersed microsystems such as micromixers (see Chapter 7) are used. They provide the desired performance and allow higher throughputs by virtue of the larger pipe diameter, but the small size of the droplets and bubbles require an additional post-reaction phase separation step [61].

In this section, the liquid–liquid slug flow MSR and its main characteristics with respect to pressure drop, RTD, heat/mass transfer and chemical reaction are presented.

15.4.2.1 **Pressure Drop**

There are two fundamental differences between gas–liquid and liquid–liquid slug flow in the MSR:

- In the liquid–liquid slug flow system, due to the close physical properties of the two fluids, it might be possible that there is no wall film and both fluids flow alternately through the capillary; this is not observed in gas–liquid systems.
- In the case of a wall film in the horizontal MSR, due to considerable shear of the discrete liquid phase on the continuous phase, the latter moves with finite velocity whereas the film in the gas–liquid system is considered stagnant.

The pressure drop in liquid–liquid slug flow comes from two main contributions: the hydrodynamic pressure drop of the individual phases and the pressure drop due to capillary phenomena. However, some studies have revealed that the liquid with superior wetting properties may form a wall film [62] which modifies the pressure drop significantly, and therefore two cases, with and without film, are considered for the theoretical prediction of the pressure drop.

In the case *without film*, if we consider the single flow unit shown in Figure 15.10a, the overall pressure drop along its length can be written as:

$$\Delta p_{\text{tot}} = \Delta p_1 + \Delta p_2 + p_{\text{C}} \tag{15.65}$$

The single-phase hydrodynamic pressure drop can be calculated using the Hagen–Poiseuille equation, whereas the capillary pressure is obtained from the Young–Laplace equation for a cylindrical tube, as follows:

$$\Delta p_1 = \frac{8\mu_1 u \alpha L_{\text{U}}}{r^2};\ \Delta p_2 = \frac{8\mu_2 u(1-\alpha) L_{\text{U}}}{r^2};\quad \text{and}\quad p_{\text{C}} = \frac{2\gamma}{r}\cos\theta_{\text{w}} \tag{15.66}$$

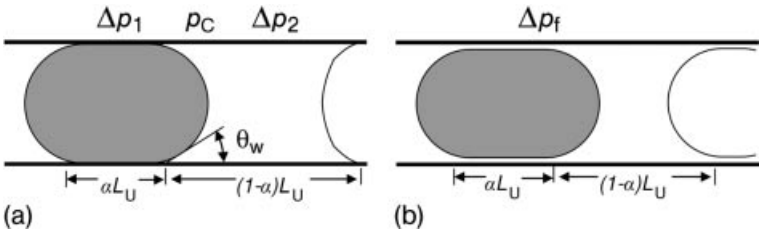

Figure 15.10 Pressure drop along a single slug unit: (a) without film and (b) with film.

where

$$u = \frac{Q_1 + Q_2}{A_{cs}}$$

and A_{cs} is the cross-sectional area of the channel.

Assuming a constant dynamic contact angle and slug lengths with an equal number of slugs of both phases under similar operating conditions and neglecting end effects, the overall pressure across a given length of the capillary is the summation of pressure drops across all slugs and the capillary pressure at all interfaces.

The major influence of the *wall film* becomes apparent when compared with single-phase slugless flow of the continuous phase. Therefore, for theoretical predictions, it is assumed that the pressure drop along the length of the capillary is due to the film region only. A model for the pressure drop in the pipeline flow of slugs (referred to as "capsules") was given by Charles [63], which relates the pressure drop in the slug region, $(\Delta p/L)_{film}$, to that of single-phase flow of the continuous phase, $(\Delta p/L)_{SP}$. According to this model, the pressure drop along the length of the film can be given by the following equation:

$$\left(\frac{\Delta p}{L_t}\right)_{film} = \left(\frac{1}{1-\kappa^4}\right)\left(\frac{\Delta p}{L_t}\right)_{SP}; \quad \kappa = \frac{R_t - \delta_{film}}{R_t} \tag{15.67}$$

In the above model, it was assumed that slugs follow each other sufficiently closely that the fluid between them can be considered as part of the slug stream. However, in the liquid–liquid slug flow for chemical engineering applications, this assumption is usually not valid and will only apply when the enclosed slug has a length several times more than the other slug. The slug which forms the film may, however, be longer depending on the inlet flow ratio for both phases. It is therefore necessary to consider the phase fraction of both liquids to calculate the pressure drop for a given length of the liquid–liquid slug flow MSR. In addition, the film thickness is very small compared with the radius of the slug, which justifies the assumption that the length of the film region for a given length of capillary is nothing more than the corresponding phase fraction times the total length. The pressure drop along the film region for a given MSR length can thus be written as

$$\frac{\Delta p}{L_t} = \left(\frac{\Delta p}{L_t}\right)_{film} = \left(\frac{\alpha}{1-\kappa^4}\right)\left(\frac{\Delta p}{L_t}\right)_{SP} \tag{15.68}$$

To calculate the pressure drop using the above equation, the film thickness is crucial. It can be estimated using Bretherton's relationship [64], as a function of capillary number, *Ca*:

$$\begin{aligned}\delta_{\text{film}} &= 1.34 R_t Ca^{2/3} \\ &= 1.34 R_t \left(\frac{\mu_2 v_{\text{slug}}}{\sigma_2}\right)^{2/3}\end{aligned} \tag{15.69}$$

In the definition of the capillary number, the slug velocity is slightly higher than the superficial flow velocity. In analogy with the theoretical predictions of Charles [63] for the pipeline flow of slugs (capsules), the slug flow and average flow velocity can be related by

$$v_{\text{slug}} = \left(\frac{2}{1+\kappa^2}\right) u \tag{15.70}$$

Power input, a decisive parameter for benchmarking technical reactors, has been investigated using the experimental pressure drop and compared with conventional contactor as shown in Table 15.5. The comparison reveals that the liquid–liquid slug flow microreactor requires much less power than the alternatives to provide large interfacial area – as high as $a = 5000\,\text{m}^2\,\text{m}^{-3}$ in a 0.5 mm capillary microreactor, which is way above the values in a mechanically agitated reactor ($a \approx 500\,\text{m}^2\,\text{m}^{-3}$).

15.4.2.2 **Residence Time Distribution**

As mentioned above, two basic situations can be envisaged in the liquid–liquid slug flow: slug with film and slug flow without film. In the case of without film, the two phases flow as distinct segments separated by each other and show ideal plug flow behavior. However, in the presence of a wall film, the reactor behaves non-ideally and two zones are formed as in gas–liquid flow. Unlike gas–liquid flow, the film also flows with finite velocity due to the considerable shear exerted by the enclosed slug on it. The behavior of the flow within the reactor can thus be evaluated by using the axial dispersion model proposed for fluid–solid systems in the above section. The

Table 15.5 Power input requirement for various liquid–liquid contactors [65].

Contactor type	Power input (kW m^{-3} of liquid)
Agitated extraction column	0.5–190
Mixer–settler	150–250
Rotating disk impinging streams contactor	175–250
Impinging streams	280
Impinging stream extractor	35–1500
Centrifugal extractor	850–2600
Liquid–liquid slug flow	0.2–20

characterization of the dispersion in the reactor should be based on the superficial velocity of the continuous phase. Thus Equation (15.6) becomes

$$C(\theta) = \frac{1}{2}\sqrt{\frac{Bo}{\pi\theta}}\exp\left[\frac{-(1-\theta)^2 Bo}{4\theta}\right] \tag{15.71}$$

where

$$C = \frac{c}{c_0}; \quad c_0 = \frac{n_{inj}}{V_R}; \quad \theta = \frac{t}{\tau}; \quad \tau = \frac{L_t}{u_L}; \quad Bo = \frac{u_L L_t}{D_{ax}}$$

15.4.2.3 **Chemical Reaction in Liquid–Liquid Systems**

In the chemical industry, a great number of reactions which are strongly exothermic are carried out on a large scale, which involve two-phase liquid–liquid systems. Thus, the intensification of heat and mass transfer is an important issue for the reactor design.

The highly exothermic and fast nitration reactions constitute an important field of application for microstructured liquid–liquid reactors (see Table 15.6). An example was given by Dummann *et al.* [66], who studied the nitration of aromatics in PTFE capillary reactors. The capillaries used had a diameter of 0.5–1 mm and a length between 1 and 4 m.

The reaction scheme is illustrated in Figure 15.11, where A is the organic material being nitrated and B is the desired mononitrated product, while C and D are dinitrated and phenolic by-products, respectively. It was shown that the phenolic product, D, is formed in parallel with the nitration of the aromatics, whereas a consecutive reaction leads to the dinitrated product, C. From kinetic studies, it is found that the activation energies of reactions (2) and (3) are higher compared with the main reaction (1). Therefore, any hot spot in the reactor will diminish the selectivity of the main product. In addition, the mass transfer between the two liquid phases must be high to increase the reactor performance and to facilitate the re-extraction of the mononitrated product into the organic phase and thus to suppress the consecutive reaction.

By adjusting the reaction conditions such as temperature, capillary length and mean residence time, the authors successfully suppressed the consecutive reaction and reduced the parallel formation of phenolic compounds to an acceptable level.

Further examples of liquid–liquid reactions carried out in microstructured reactors are summarized in Table 15.6.

Chemical reactions have also been used as a tool to characterize the mass transfer in MSR.

As pointed out, common modes of interface in the case of liquid–liquid two-phase flow are “slug flow” and “parallel flow” (Figure 15.9). In the case of slug flow, two mechanisms are known to be responsible for the mass transfer between the two liquids: (a) internal circulation [66, 75, 84] takes place within each slug and (b) the concentration gradients between adjacent slugs lead to the diffusion between the phases . In the case of the parallel pattern, the flow is laminar and the transfer of molecules between the two phases is supposed to occur only by diffusion.

Table 15.6 Examples of liquid–liquid reactions studied in MSRs.

Reaction	Reactor	Reference
Nitration of benzene	Stainless-steel and PTFE capillary MSR	Dummann *et al.* [66]; Burns and Ramshaw [67, 68]
Nitration of benzene	Borosilicate glass microreactor	Doku *et al.* [69]
Nitration of toluene	PTFE capillary MSR	Burns and Ramshaw [68]
Transesterification – production of alkyl esters	PTFE capillary MSR	Jachuck [70]
Vitamin precursor synthesis – production of β-ionone	Microreaction system with 32 parallel reaction channels	Wörz and co-workers [70–72]
Hydrolysis of *p*-nitrophenol acetate	PMMA microreactor and PTFE tubing	Ahmed *et al.* [73]; Ahmed-Omer [74]
Tandem diazotation/Heck reaction sequences	PMMA microreactor	Ahmed *et al.* [73]
Titration reaction	Soda-lime glass etched with rectangular channels	Burns and Ramshaw [75]
Titration reaction	PTFE capillary MSR	Kashid [65]
Titration reaction	Rectangular glass MSR	Dessimoz *et al.* [76]
Nitration of toluene, nitration of dialkyl-substituted thioureas	Silicon microreactor with nine reactor channels	Antes *et al.* [77]
Villermaux–Dushman – instantaneous neutralization and rapid redox reactions	PDMS MSR	Matsuyama *et al.* [78]
Bromination of styrene	Thiolene-based resin MSR device	Cygan *et al.* [79]
Extraction and detection of carbaryl derivative	Two Pyrex glass MSRs	Smirnova *et al.* [80]
Degradation of *p*-chlorophenol	Pyrex glass MSR	Maruyama *et al.* [81]
Kinetics of ribonuclease A (RNase A)	PDMS MSR	Song and Ismagilov [82]
Hydrolysis of *p*-nitrophenyl acetate	PTFE MSR	Ahmed-Omer [74]
Phase-transfer alkylation of β-keto esters	Microchip connected to a Teflon tube	Ueno *et al.* [83]

Several workers have used fast chemical reactions to determine the global mass transfer coefficient (k_{gl}) in microstructured liquid–liquid reactors [75, 76]. The neutralizations of trichloroacetic acid [76] [Equation (15.72)] and acetic acid [75] were used as model reactions. The reactions are instantaneous and, therefore, are controlled by mass transfer.

$$CCl_3COOH_{or} + NaOH_{aq} \rightarrow CCl_3COO^- Na_{aq}^+ + H_2O \qquad (15.72)$$

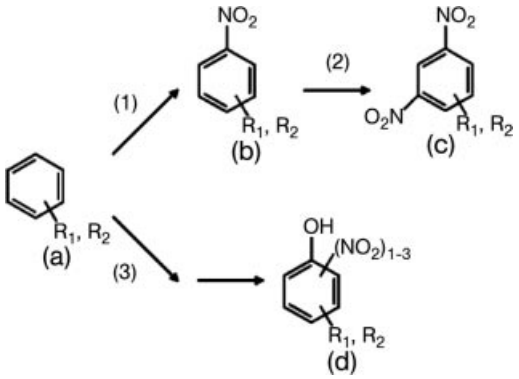

Figure 15.11 Nitration of single-ring aromatics.

In Table 15.7, the experimentally obtained global volumetric mass transfer coefficients are summarized and compared with gas–liquid systems and conventional liquid–liquid contactors. It should be mentioned that the flow regime in capillary reactors is very sensitive to the physical properties of the two liquids. The formation of slug and parallel flow is controlled by the competition between viscous forces and interfacial tension. As the physical properties can change during the extraction and reaction in the capillary, the flow pattern may also change and, as a consequence, modify the mass transfer processes.

For slug flow, the volumetric mass transfer coefficient increases with the superficial velocity. Neglecting the contribution of the wall film to the mass transfer, the specific area of a slug is given by

$$a \cong \frac{2{d_t}^2}{{d_t}^2 L_s} = \frac{2}{L_s} \tag{15.73}$$

Therefore, the volumetric mass transfer coefficient is supposed to be inversely proportional to the slug length in the capillary. This was confirmed experimentally by Burns and Ramshaw [75] and Kashid [65], who found the following relationship:

$$k_{gl}a \sim 0.3\, u^{0.2-0.94} L_s \tag{15.74}$$

15.5 Three-phase Reactions

15.5.1 Gas–Liquid–Solid

Most of the reported microstructured gas–liquid–solid reactors concern catalytic hydrogenation (Table 15.8). This is because hydrogenation reactions represent about 20% of all the reaction steps in a typical fine chemical synthesis. Catalytic

Table 15.7 Comparison of mass transfer data for microsystems and conventional contactors [76].

Reference	Regime and system	Conditions	Global volumetric mass transfer coefficient
Liquid–liquid system in microreactors			
Burns and Ramshaw (2001)	• *Slug flow* • *Reacting system* Kerosene–acetic acid–water + NaOH	$d_H = 380\,\mu m$ $C_{acetic\ acid,\ org} = 0.65\ M$ $C_{NaOH,aq} = 0.1–0.4\ M$ $u = 0–35\ mm\ s^{-1}$	Order of magnitude of $0.5\ s^{-1}$
Kashid *et al.* (2007)	• *Slug flow* • *Non-reacting system* Kerosene–acetic acid–water	$d = 0.5–1\ mm$ $C_{acetic\ acid,\ org} = 0.03\ M$ $u = 10–30\ mm\ s^{-1}$ $u = 30–70\ mm\ s^{-1}$	$\sim 0.4 - 0.8\ s^{-1}$ $\sim 0.8 - 1.4\ s^{-1}$
Dessimoz *et al.* [76]	• *Slug flow* • *Reacting system* Hexane–trichloroacetic acid–water + NaOH	$d_H = 400\,\mu m$ $C_{acid,\ org} = 0.6\ M$ $C_{NaOH,aq} = 0.15–0.3\ M$ $u = 0–20\ mm\ s^{-1}$	$0.2 - 0.5\ s^{-1}$
Dessimoz *et al.* [76]	• *Parallel flow* • *Reacting system* Toluene–trichloroacetic acid–water + NaOH	$d_H = 269\,\mu m$ $C_{acid,\ org} = 0.6\ M$ $C_{NaOH,aq} = 0.1–0.2\ M$ $u = 0–50\ mm\ s^{-1}$	$0.2 - 0.5\ s^{-1}$

(*Continued*)

Table 15.7 (*Continued*)

Reference	Regime and system	Conditions	Global volumetric mass transfer coefficient
Gas–liquid system in microreactors			
Yue *et al.* [43]	• *Slug flow* • *Reacting system* CO_2–buffer solution of $NaHCO_3$, Na_2CO_3, NaOH	$d_H = 669\,\mu m$ $u_G = 0–2\,m\,s^{-1}$ $u_L = 0.09–1\,m\,s^{-1}$	Liquid side volumetric mass transfer coefficient in the order of $0.3 - 0.5\,s^{-1}$ ($u_L = 0.09\,m\,s^{-1}$)
Conventional contactors for liquid–liquid systems [62]			
Spray column	• *Non-reacting system* Water–acetic acid–benzene		$\sim 1.75 - 6.3) \times 10^{-3}\,s^{-1}$
Impinging streams	• *Non-reacting system* Kerosene–acetic acid–water		$0.05 - 0.3\,s^{-1}$

Table 15.8 Examples of gas–liquid–liquid reactions studied in MSRs.

Reaction	Reactor	Reference
Hydrogenation of cyclohexene	Micropacked bed reactor and microchannel with staggered arrays columns	Losey and co-workers [86, 87]
Hydrogenation of nitrobenzene	Falling film MSR	Yeong *et al.* [88]
Hydrogenation of *p*-nitrotoluene	MSR made of stack of aluminum wafers	Födisch *et al.* [89]
Hydrogenation of α-methylstyrene	Micropacked bed reactor	Losey *et al.* [90]
Hydrogenation of α-methylstyrene	Microstructured mesh contactor	Abdallah *et al.* [37]

hydrogenations are fast and highly exothermic reactions. Consequently, reactor performance and product selectivity are strongly influenced by mass transfer and heat evacuation is an important issue. Both problems may be overcome using microstructured devices.

Different types of gas–liquid–solid MSRs have been developed, using different gas–liquid contacting principles (see Chapter 8) [85]. These principles can be classified as follows:

- Continuous-phase contacting, where the fluid phases are separated. Examples are microstructured falling film and mesh reactors.
- Dispersed-phase contacting, obtained when one of the fluid phases is dispersed into the other phase.

Regular flow patterns are provided by the segmented flow in a single capillary or in multi-channel microreactors. Miniaturized packed-bed microreactors follow the paths of classical engineering by enabling trickle-bed or packed bubble column operation. Most of the microstructured multiphase reactors are at the research stage. Due to the small reaction volumes they will find their application mainly in small-scale production in the fine chemical and pharmaceutical industries.

15.5.1.1 Continuous-phase Microstructured Reactors

In *falling film contactors*, a thin film is created by a liquid falling under gravity pull. The liquid flows over a solid support, which is normally a thin wall or stack of pipes. In conventional falling film devices, a film with a thickness of 0.5–3 mm is generated [85]. This rather thick liquid film results in an important mass transfer resistance for the gaseous reactant diffusing to the solid catalyst on the reactor wall. In addition, the film flow becomes unstable at high throughput and the film may break up into rivulets, fingers or a series of droplets. The mentioned problems can be overcome by microstructuring the solid wall [30, 91]. The microstructured falling film reactor consists of microchannels, which are typically 300 μm wide, 100 μm deep and ~80 mm long. The channels are separated by 100 μm wide walls.

Yeong *et al.* [88, 92] used a microstructured film reactor for the hydrogenation of nitrobenzene to aniline in ethanol at 60 °C, 0.1–0.4 MPa hydrogen pressure and a residence time of 9–17 s. Palladium catalyst was deposited as films or particles on the microstructured plate. Confocal microscopy was used to measure the liquid film thickness. With increasing flow rate between 0.5 and 1.0 $cm^3\,min^{-1}$, thicker liquid films between 67 and 92 μm were observed. The k_La of this system was estimated to be 3–8 s^{-1} with an interfacial surface area per reaction volume of 9000–15 000 $m^2\,m^{-3}$. Conversion was found to be affected by both liquid flow rate and hydrogen pressure and the reactor operated between the kinetic- and mass transfer-controlled regimes.

The main drawback of the microstructured falling film reactor is the residence time of the liquid in the channels, which is in the range of 5–20 s, depending on the physical properties of the liquid and the operating conditions. The residence time can be increased by prolonging the channels or by decreasing the angle of descent, which can be achieved with a helicoidal microchannel falling film reactor. For a microchannel with a small angle descent of 7.5° the residence time could be increased by a factor of ∼50 [93].

In a *mesh microcontactor*, the gas and liquid flow through separate channels. To provide stable operation, the fluid interface is immobilized by well-defined openings obtained with a thin mesh [94]. Interfacial forces help to stabilize the fluid interface within the openings, while fluid layers are thin enough to enhance mass transfer.

The meniscus shape at the interface between the two phases defines the available area for mass transfer and is a function of contact angle, pore geometry and pressure difference between phases. The open area of the micromesh contactor is about 20–25%, which leads to a gas–liquid interfacial area of 2000 $m^2\,m^{-3}$, well above the values obtained in traditional stirred tank reactors. This high gas–liquid interfacial area combined with the small fluid layer thickness resulted in high mass transfer coefficients. Abdallah and co-workers [37, 95] estimated the volumetric mass transfer coefficients, k_La_L, during the very fast hydrogenation of α-methylstyrene over a Pd/γ-alumina catalyst. The global gas–liquid–solid volumetric mass transfer coefficient, k_La, measured experimentally was in the range 0.8–1.6 s^{-1}. These values are well above those predicted by the film model and those obtained from a CFD (3D model) simulation.

15.5.1.2 **Dispersed-phase Microstructured Reactors**

In *segmented flow gas–liquid–solid reactors*, the liquid usually flows over the solid surface while the gas flows through the liquid in the form of bubbles or annular flow, depending on the MSR geometry and the catalyst arrangement.

The hydrodynamic characteristics of three-phase reactors, such as pressure drop and residence time distribution, can be determined from those for fluid–solid and fluid–fluid reactors. The difference between the gas–liquid and gas–liquid–solid systems is that due to the reaction at the surface of the catalyst, there is always a concentration gradient in the liquid phase in the latter case. Unlike in gas–liquid reactions, it is always important to saturate the liquid film with the gaseous

component. To ensure constant saturation, the following criterion has to be satisfied:

$$\frac{L_b D_m}{\nu_b \delta^2} \gg 1 \tag{15.75}$$

The global transformation rate of a gas–liquid reaction catalyst by a solid catalyst is influenced by the mass transfer between the gas–liquid and the liquid–solid mass transfer. Mass transfer and surface reaction are in series and, for fast chemical reactions, mass transfer will influence the reactant concentration on the catalytic surface and, as a consequence, influence the reactor performance and the product selectivity. For the gaseous reactant three mass transfer steps can be identified [96]: (1) the transfer from the bubble through the liquid film to the catalyst ($k_{GS}a_{GS}$), (2) the transfer from the caps of the gas bubbles to the liquid slug ($k_{GS}a_{GS}$) and (3) the transfer of dissolved gas to the catalytic surface ($k_{LS}a_{LS}$) . Steps 2 and 3 are in series and in parallel with respect to step 1, respectively. The following expression describes the overall mass transfer ($k_{ov}a$):

$$k_{ov}a = k_{GS}a_{GS} + \left(\frac{1}{k_{GL}a_{GL}} + \frac{1}{k_{LS}a_{LS}}\right)^{-1} \tag{15.76}$$

Different attempts were made to determine the mass transfer coefficient separately in non-reactive systems. However, the concentration profiles in the liquid surface film and in the slugs are strongly affected by fast chemical reactions and the results must be interpreted with caution.

As hydrogenations are fast and highly exothermic reactions, the heat of reaction must be effectively evacuated to ensure isothermal operation and to avoid reaction runaway. An efficient device for this purpose was proposed by Hessel *et al.* [2]. The authors arranged the microchannels in parallel in between cooling channels as shown in Figure 15.12. Each channel worked under segmented flow conditions. The main problem to overcome is the uniform distribution of both gas and liquid flow over the microchannels to ensure identical flow behavior and residence time.

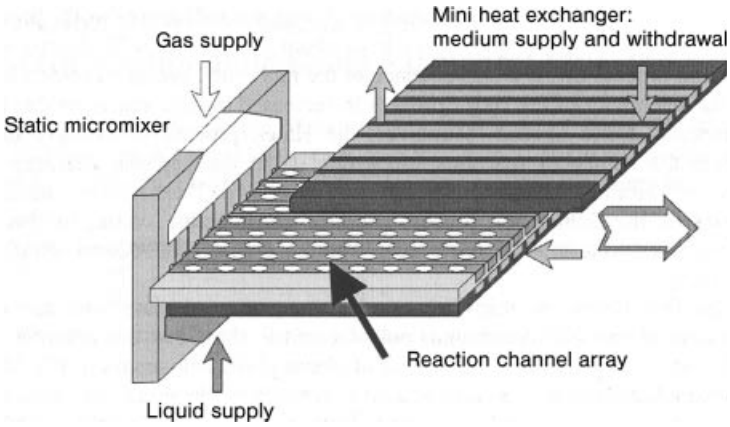

Figure 15.12 Microbubble column with integrated cooling channels [2].

Many reported microreactors used for gas–liquid–solid reactions are *micropacked beds*. An advantage of microstructured packed beds for hydrogenation processes stems from the fact that active and selective catalysts are commercially available. In addition, the particle size of these catalysts used in suspension reactors is in the micrometer range and fits well for use in microchannels. However, proper design of the reactor is required to maintain an acceptable pressure drop. To avoid an excessive pressure drop, Losey *et al.* [87] constructed a microchemical system consisting of a microfluidic distribution manifold and a microchannel array. Multiple reagent streams (specifically, gas and liquid streams) were mixed on-chip and the fluid streams were brought into contact by a series of interleaved, high aspect ratio inlet channels. These inlet channels deliver the reactants continuously and cocurrently to 10 reactor chambers containing standard catalytic particles with diameters in the range 50–75 μm. Flow regimes in the microreactor were characterized visually for different flow rates and gas-to-liquid flow ratios. For low liquid and gas velocities, bubbles were formed at the entrance and were carried by the liquid through the packed bed. Under these conditions, the hydrogenation of cyclohexene was studied and used as a model reaction to measure the mass transfer resistances. Overall mass transfer coefficients ($k_{ov}a$) were measured to range from 5 to 15 s^{-1}, which is nearly two orders of magnitude larger than values reported in the literature for standard laboratory-scale reactors.

Increasing flow velocities in the microreactor lead to pulsations and the formation of segmented flow. The different flow patterns observed in microstructured packed beds were studied in detail by van Herk *et al.* [98]. They confirmed the segregated flow pattern at high gas fractions.

More recently, the catalytic hydrogenation of *o*-nitroanisole in a microstructured packed bed reactor was studied by Tadepalli *et al.* [99]. The reactor had an inner diameter of 0.775 mm and was filled with Pd/zeolite catalyst with particle diameters in the range 45–75 and 75–150 μm. The length of the catalytic bed could be varied between 60 and 80 mm. It was stated that segmented gas–liquid flow was observed, but, further hydrodynamic studies are missing.

To increase mass transfer in solid catalyzed gas–liquid hydrogenations, the reactions are often operated at high pressures. Silicon/glass microreactors present a possibility to handle high-pressures safely and provide optical access into the reaction channel for flow investigations. Trachsel *et al.* [100] reported an Si/glass microreactor with soldered microfluidic connections for high-pressure and high-temperature applications. Mechanical testing of the device by tensile and pressure tests showed no failure for continuous operation at 14 MPa and 80 °C. The microreactor design was applied to the well-described solid catalyzed exothermic hydrogenation of cyclohexene at operating conditions up to 5.1 MPa and 71 °C.

15.5.2 Gas–Liquid–Liquid Systems

Gas–liquid–liquid reactions have several applications, such as hydroformylation, carbonylation, hydrogenation, oligomerization, polymerization, hydrometallurgical

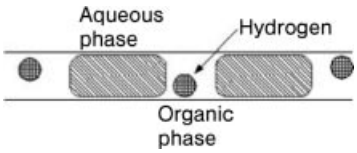

Figure 15.13 Schematics of gas–liquid–liquid flow patterns observed in the selective hydrogenation of α,β-unsaturated aldehydes. Adapted from Önal *et al.* [102].

processes, biochemical processes and fine chemical manufacture. Developments in homogeneous catalysis have made these reaction systems increasingly attractive in recent years. Gas–liquid–liquid systems are encountered in reaction systems that comprise three phases of two (or more) immiscible reactants, reaction products or catalyst [101]. In some cases, the three reactants are supplied from three different phases (e.g. Koch reaction). It is also possible to intensify the mass transfer in a liquid–liquid system; additional gas phase may be added to enhance mixing and augment the interfacial area.

The flow patterns of gas–liquid–liquid flow in the MSR depend on the volume fraction of each phase within the reactor. At low gas volume fractions, the gas remains in one of the liquids while both liquids flow in the form of slugs. If the reaction is mass transfer limited, the overall reaction rate is strongly dependent on the interfacial liquid–liquid mass transfer. By reducing the capillary diameter, the specific interfacial area increases and leads to an intensified process.

Önal *et al.* [102] carried out the selective hydrogenation of α,β-unsaturated aldehydes in aqueous solution using a PTFE capillary of diameter 500–1000 μm. The gas–liquid–liquid flow observed in the reactor is depicted in Figure 15.13. This shows the alternate flow of two liquid phases with the organic forming a wall film due to its affinity towards the capillary material and hydrogen in the form of small bubbles in the organic phase. The reaction rate showed a significant effect of global reaction rates with a three-fold increase on reducing the channel diameter from 1000 to 500 μm.

15.6 Conclusion

In this chapter, the various characteristics of multiphase MSRs are presented. It is clear that MSRs are most suitable for reactions which have fast intrinsic kinetics and require rapid transport, high temperatures and inherent safety. Effective exploitation of the full chemical potential of catalysts through high rates of heat and mass transfer provides an excellent means for identifying novel synthesis routes which are both economically attractive and environmentally benign.

The time available for chemical transformation in the microreactors is very short due to their small size, which results in low hold-ups on the one hand, but necessitates highly efficient mass/heat transfer on the other. The amount of power

dissipation for multiphase reactions per unit interfacial area is very low in MSRs, leading to significant reductions in the energy consumption as a further environmental benefit. The well-defined flow patterns in fluid–fluid and three-phase reactors mean that the reactions can be controlled precisely, which eliminates stochastic effects and permits not only high mass and heat transfer rates but also precise control of residence time and RTD to produce chemicals with higher specifications.

Nevertheless, there are several constraints that hamper the use of microreactors for multiphase reactions. In the catalytic MSR, the performance is very adversely affected by catalyst deactivation. Effective *in situ* catalyst regeneration therefore becomes necessary, since the simple catalyst change practiced in conventional reactors is usually no longer an option. The thickness of the microreactor catalytic wall is often greater than the internal diameter of the channel and, therefore, may impede heat transfer for highly exothermic reactions, leading to non-isothermal behavior. Reactions involving highly viscous materials or suspended particles are difficult to carry out in the microreactor. Moreover, the reliable modeling of such systems at the microscale is still poorly developed. Last, but very important, reliable numbering up needs to be resolved. If one fails to achieve a uniform distribution over parallel microstructured elements, many of the advantages of MSRs are forfeited. Advanced CFD techniques have had only limited success in providing a solution to this fundamental question related to the large-scale application of MSRs.

List of Symbols

A	Cross-sectional area	m^2
a	Specific interfacial area	$m^2\,m^{-3}$
A_b	Cross-sectional area of bubble	m^2
Bo	Bodenstein number	–
c, c_i,c_{ib},c_{is}	Concentration, concentration of compound i, concentration of compound i in bulk, concentration of compound i on catalyst surface	$mol\,m^{-3}$
c_0	Initial concentration	$mol\,m^{-3}$
c_{dyn}, c_{st}	Concentration of tracer in dynamic and static liquid region	$mol\,m^{-3}$
c_s	Reactant concentration on the outer catalyst surface	$mol\,m^{-3}$
$C(\theta)$	Reference tracer concentration	–
d_t, d_h	Diameter of the channel (tube), hydraulic diameter	m
D_m	Molecular diffusion coefficient	$m^2\,s^{-1}$
D_{eff}	Effective diffusion coefficient	$m^2\,s^{-1}$
d_p	Diameter of particle	m

D_{ax}	Axial dispersion coefficient	$m^2\,s^{-1}$
E	Activation energy	$J\,mol^{-1}$
f, f_E	Friction factor, two-phase friction factor	–
g	Gravitational acceleration	$m\,s^{-2}$
H	Height of rectangular channel	m
h	Heat transfer coefficient	$W\,m^{-2}K^{-1}$
J_{ji}	Molar flux of jth component in ith phase	$mol\,m^{-2}s^{-1}$
k_s	Intrinsic rate constant, surface reaction	s^{-1}
k_r	Intrinsic rate constant	Variable
k_G, k_L	Mass transfer coefficient (gas, liquid phase)	$m\,s^{-1}$
k_Ga, k_La	Volumetric mass transfer coefficient of gas from bulk liquid to catalyst surface	s^{-1}
k_{gl}	Global mass transfer coefficient	$m\,s^{-1}$
$k_{L,cap}$, $k_{L,film}$	Coefficient of mass transfer for a solute transferring through hemispherical cap and film, respectively	$m\,s^{-1}$
L, L_t	Length, channel length	m
L_e	Length of entrance zone	m
L_{bed}	Length of bed	m
L_s, L_b	Length of the slug (liquid), length of bubble	m
L_{UC}	Length of a unit cell (a pair of gas and liquid slugs in gas–liquid flow and two liquid slugs in liquid–liquid flow)	m
N	Number of parallel channels	–
n	Order of reaction	–
n_{inj}	Number of moles injected	mol
p_c	Capillary pressure	Pa
Pe	Peclet number	–
Q Q_i	Volumetric flow rate, volumetric flow through i^{th} channel	$m^3\,s^{-1}$
R	Gas constant	$J\,mol^{-1}\,K^{-1}$
Re	Reynolds number	–
R_t	Radius of tube/microreactor	m
R_b	Radius of bubble	m
s	Slip	–
Sh, Sc	Sherwood number, Schmidt number	–

r_0, r_1	Radial position of vortex center and dividing streamline	m
r_{eff}	Observed effective reaction rate	$mol\,m^{-3}\,s^{-1}$
r_s	Reaction rate at catalyst surface	$mol\,m^{-2}\,s^{-1}$
T_s	Temperature at catalyst surface	K
t	Time	s
u, u_G, u_L, u_e, u_{dyn}	Superficial velocity, of gas, of liquid, gravity equivalent velocity, velocity of recirculating region	$m\,s^{-1}$
v_b, v_{slug}	Velocity of bubble, of slug	$m\,s^{-1}$
V_R, V_i	Volume of reactor, volume of i^{th} channel	m^3
W	Width of rectangular channel	m
X	Conversion	–
z	Cartesian coordinate	m
ΔH_R	Reaction enthalpy	J
Δp, Δp_f	Pressure drop, frictional pressure drop	Pa
Δp_U, Δp_H	Pressure drop over slug unit (a pair of two liquid slugs) and hydrodynamics pressure drop	Pa
Δp_{tot}, Δp_1, Δp_2	Total pressure drop, pressure drop due to phase 1, due to phase 2 respectively	Pa
$(\Delta p_f/\Delta z)_G$, $(\Delta p_f/\Delta z)_L$	Frictional pressure gradient, gas and liquid	$Pa\,m^{-1}$
$(\Delta p_f/\Delta z)_{2p}$	Two-phase pressure gradient	$Pa\,m^{-1}$
$(\Delta p/L_t)_{film}$	Pressure gradient due to film region	$Pa\,m^{-1}$
$(\Delta p/L_t)_{SP}$	Pressure gradient of single phase flow flowing through same microreactor of film flow	$Pa\,m^{-1}$
ϕ	Fraction of liquid in the dynamic phase	–
Φ_G^2, Φ_L^2	Friction multipliers	–
α	Volume fraction of liquid phase which flows in the form of enclosed slug (discrete phase)	–
γ	Interfacial tension	$N\,m^{-1}$
ζ, χ	Geometric factors	–
δ_{film}	Film thickness	m
δ_{cat}	Thickness of porous catalytic layer	m
η_{ex}	External effectiveness factor	–

θ	Dimensionless time ($= t/\tau$)	–
θ_w	Three-phase contact angle	°
λ	Eigenvalues of the infinite series solution	–
λ_{eff}	Thermal conductivity of the porous catalyst	$W\,m^{-1}\,K^{-1}$
ϵ	Porosity of bed	–
ε_G, ε_L	Gas, liquid	–
μ	Dynamic viscosity	$kg\,m^{-1}\,s^{-1}$
ρ	Density	$kg\,m^{-3}$
σ_d	Standard deviation	–
τ	Residence time, space time	s
Ψ	Lockhart–Martinelli parameter	–

References

1 W. Bier, W. Keller, G. Linder, D. Seidel, K. Schubert and H. Martin, Gas to gas heat-transfer in micro heat-exchangers. *Chemical Engineering Processing*, **1993**, *32* (1), 33–43.

2 V. Hessel, W. Ehrfeld, K. Golbig, V. Haverkamp, H. Löwe, M. Storz and C. Wille, Gas/liquid microreactors for direct fluorination of aromatic compounds using elemental fluorine, in *Proceedings of the 3rd International Conference on Microreaction Technology (IMRET3)*, ed. W. Ehrfeld, Springer, Berlin, **1999**, 526–540.

3 M. Grunewald and D. W. Agar, Intensification of regenerative heat exchange in chemical reactors using desorptive cooling. *Industrial and Engineering Chemistry Research*, **2004**, *43* (16), 4773–4779.

4 M. M. Sharma and A. K. Nanda, Extraction with second order reaction. *Transactions of the Institution of Chemical Engineers and the Chemical Engineer*, **1968**, *46* (2), T44.

5 Y. T. Shah, *Gas Liquid Solid Reactor Design*, McGraw-Hill, New York, **1979**.

6 M. Baerns and A. Renken, Chemische Reaktionstechnik, in *Winnacker-Küchler: Chemische Technik: Prozesse und Produkte*, Wiley-VCH Verlag GmbH, Weinheim, **2004**, 453–643.

7 O. Levenspiel, *Chemical Reaction Engineering*, 3rd edn, John Wiley and Sons, Inc., New York, **1999**.

8 L. Kiwi-Minsker and A. Renken, Microstructured catalytic reactors, in *Handbook of Heterogeneous Catalysis* G. Ertl, *et al.*, Wiley-VCH Verlag GmbH, Weinheim, **2008**, 2248–2264.

9 V. Meille, Review on methods to deposit catalysts on structured surfaces. *Applied Catalysis A: General*, **2006**, *315*, 1–17.

10 J.-M. Commenge, L. Falk, J.-P. Corriou and M. Matlosz, Optimal design for flow uniformity in microchannel reactors. *AIChE Journal*, **2002**, *48* (2), 345–358.

11 Verein Deutscher Ingenieure, *VDI-Wärmeatlas*, 9th edn, Springer, Berlin, **2002**.

12 A. Rouge, *Periodic Operation of a Microreactor for Heterogeneously Catalyzed Reactions: the Dehydration of Isopropanol*, PhD EPFL, Lausanne, **2001**.

13 M. Günther, S. Schneider, J. Wagner, R. Gorges, T. Henkel, M. Kielpinski, J. Albert, R. Bierbaum and J. M. Kohler, Characterization of residence time and

residence time distribution in chip reactors with modular arrangements by integrated optical detection. *Chemical Engineering Journal*, **2004**, *101* (1–3), 373–378.

14 F. Trachsel, A. Günther, S. Khan and K. F. Jensen, Measurement of residence time distribution in microfluidic systems. *Chemical Engineering Science*, **2005**, *60* (21), 5729–5737.

15 D. Boskovic and S. Loebbecke, Modelling of the residence time distribution in micromixers. *Chemical Engineering Journal*, **2008**, *135* S138–S146.

16 D. E. Mears, Tests for transport limitations in experimental catalytic reactors. *Industrial and Engineering Chemistry Process Design and Development*, **1971**, *10* (4), 541.

17 G. Taylor, Dispersion of soluble matter in solvent flowing slowly through a tube. *Proceedings of the Royal Society of London, Series A*, **1953**, *A219*, 186–203.

18 R. Aris, On the dispersion of a solute in a fluid flowing through a tube. *Proceedings of the Royal Society of London, Series A*, **1956**, *A235*, 67–77.

19 J. M. Commenge, A. Rouge, A. Renken, J. P. Corriou and M. Matlosz, Dispersion dans un microréacteur multitubulaire. Etude expérimentale et modélization. *Récents Progrés en Génie des Procédés*, **2001**, *15*, 329–336.

20 A. Rouge and A. Renken, Performance enhancement of a microchannel reactor under periodic operation. *Studies in Surface Science and Catalysis*, **2001**, *133*, 239–246.

21 E. R. Delsman, M. H. J. M. De Croon, A. Pierik, G. J. Kramer, P. D. Cobden, C. Hofmann, V. Cominos and J. C. Schouten, Design and operation of a preferential oxidation microdevice for a portable fuel processor. *Chemical Engineering Science*, **2004**, *59* (22–23), 4795–4802.

22 M. J. M. Mies, E. V. Rebrov, M. H. J. De Croon, J. C. Schouten and I. Z. Ismagilov, Inlet section for providing a uniform flow distribution in a downstream reactor comprises upstream and downstream passage with specifically positioned elongated parallel upstream and downstream channels. **2006**, WO2006107206-A2.

23 E. R. Delsman, M. H. J. M. de Croon, G. D. Elzinga, P. D. Cobden, G. J. Kramer and J. C. Schouten, The influence of differences between microchannels on microreactor performance. *Chemical Engineering and Technology*, **2005**, *28* (3), 367–375.

24 E. R. Delsman, B. Laarhoven, M. de, Croon G. J. Kramer and J. C. Schouten, Comparison between conventional fixed-bed and microreactor technology for a portable hydrogen production case. *Chemical Engineering Research and Design*, **2005**, *83* (A9), 1063–1075.

25 D. F. Sherony and C. W. Solbrig, analytical investigation of heat or mass transfer and friction factors in a corrugated duct heat or mass exchanger. *International Journal of Heat and Mass Transfer*, **1970**, *13* (1), 145.

26 J. H. B. J. Hoebink and G. B. Marin, Modeling of monolihic reactors for automotive exhaust gas treatment in *Structured Catalysts and Reactors*, ed. J. A. M. A. Cybulski, Marcel Dekker, New York, **1998**.

27 A. Cybulski and J. A. Moulijn, Monoliths in heterogeneous catalysis. *Catal. Rev. Sci. Eng.*, **1994**, *36* (2), 179–270.

28 R. E. Hayes and S. T. Kolaczkowski, Mass and heat transfer effects in catalytic monolith reactors. *Chemical Engineering Science*, **1994**, *49* (21), 3587–3599.

29 J. Villermaux, Diffusion dans un reacteur cylindrique. *International Journal of Heat and Mass Transfer*, **1971**, *14* (12), 1963–1981.

30 K. Jähnisch, M. Baerns, V. Hessel, W. Ehrfeld, V. Haverkamp, H. Löwe, C. Wille and A. Guber, Direct fluorination of toluene using elemental fluorine in gas/liquid microreactors. *Journal of Fluorine Chemistry*, **2000**, *105* (1), 117–128.

31 R. D. Chambers, D. Rolling, R. C. H. Spink and G. Sandford, Elemental fluorine. Part 13: gas–liquid thin film microreactors for selective direct

fluorination. *Lab on a Chip*, **2001**, *1* (2), 132–137.

32 D. Wehle, M. Dejmek, J. Rosenthal, H. Ernst, D. Kampmann, S. Trautschold and R. Pechatschek, *Chlorinated Organic Compound Production,* Clariant GmbH, WO200210094-A.

33 H. Ehrich, D. Linke, K. Morgenschweis, M. Baerns and K. Jähnisch, Application of microstructured reactor technology for the photochemical chlorination of alkylaromatics. *Chimia*, **2002**, *56* (11), 647–653.

34 J. Antes, T. Tuercke, J. Kerth, E. Marioth, F. Schnuerer, H. H. Krause and S. Loebbecke, Use of microreactors for nitration processes, in *4th International Conference on Microreaction Technology (IMRET 4), Atlanta, GA*, **2001**.

35 R. D. Chambers, D. Holling, A. J. Rees and G. Sandford, Microreactors for oxidations using fluorine. *Journal of Fluorine Chemistry*, **2003**, *119* (1), 81–82.

36 A. Müller, V. Cominos, V. Hessel, B. Horn, J. Schürer, A. Ziogas, K. Jähnisch, V. Hillmann, V. Grosser, K. A. Jam, A. Bazzanella, G. Rinke and M. Kraut, Fluidic bus system for chemical process engineering in the laboratory and for small-scale production. *Chemical Engineering Journal*, **2005**, *107* (1–3), 205–214.

37 R. Abdallah, V. Meille, J. Shaw, D. Wenn and C. De Bellefon, Gas–liquid and gas–liquid–solid catalysis in a mesh microreactor. *Chemical Communications*, **2004**, 372–373.

38 E. P. Van Elk, P. C. Borman, J. A. M. Kuipers and G. F. Versteeg, Modelling of gas–liquid reactors – implementation of the penetration model in dynamic modelling of gas–liquid processes with the presence of a liquid bulk. *Chemical Engineering Journal*, **2000**, *76* (3), 223–237.

39 E. P. van Elk, Gas–liquid reactions – influence of liquid bulk and mass transfer on process performance, *PhD Thesis*, University of Twente, **2001**.

40 N. Kockmann, Transport phenomena in micro process enginnering, in *Heat and Mass Transfer*, ed. D. Mewes and F. Mayinger, Springer, Berlin, **2008**, 122–123.

41 R. W. Lockhart and R. C. Martinelli, Proposed correlation of data for isothermal 2-phase, 2-component flow in pipes. *Chemical Engineering Progress*, **1949**, *45* (1), 39–48.

42 D. Chisholm, A theoretical basis for Lockhart–Martinelli correlation for 2-phase flow. *International Journal of Heat and Mass Transfer*, **1767**, *10* (12), 1967.

43 J. Yue, G. W. Chen, Q. Yuan, L. G. Luo and Y. Gonthier, Hydrodynamics and mass transfer characteristics in gas–liquid flow through a rectangular microchannel. *Chemical Engineering Science*, **2007**, *62* (7), 2096–2108.

44 I. Y. Chen, K. S. Yang and C. C. Wang, An empirical correlation for two-phase frictional performance in small diameter tubes. *International Journal of Heat and Mass Transfer*, **2002**, *45* (17), 3667–3671.

45 H. Liu, C. O. Vandu and R. Krishna, Hydrodynamics of Taylor flow in vertical capillaries: flow regimes, bubble rise velocity, liquid slug length and pressure drop. *Industrial and Engineering Chemistry Research*, **2005**, *44* (14), 4884–4897.

46 J. N. Tilton, Fluid and particle dynamics, in *in Perry's Chemical Engineers' Handbook*, ed. R. H. Perry, D. W. Green and J. O. Maloney, McGraw-Hill, New York, **1997**, section 6, 1–54.

47 M. Kreutzer, Hydrodynamics of Taylor flow in capillaries and monolith reactors, *PhD Thesis*, Delft University of Technology, **2003**.

48 T. C. Thulasidas, M. A. Abraham and R. L. Cerro, Bubble-train flow in capillaries of circular and square cross-section. *Chemical Engineering Science*, **1995**, *50* (2), 183–199.

49 T. C. Thulasidas, M. A. Abraham and R. L. Cerro, Dispersion during bubble-train flow in capillaries. *Chemical Engineering Science*, **1999**, *54* (1), 61–76.

50 P. Aussillous and D. Quere, Quick deposition of a fluid on the wall of a

tube. *Physics of Fluids*, **2000**, *12* (10), 2367–2371.

51 W. G. Whitman, Preliminary experimental confirmation of the two-film theory of gas absorption. *Chem. Metall. Eng.*, **1923**, *29*, 146–148.

52 R. Higbie, The rate of absorption of a pure gas into a still liquid during short periods of exposure. *Transactions of the American Institute of Chemical Engineers*, **1935**, *31*, 365–389.

53 P. V. Danckwerts, Significance of liquid-film coefficients in gas absorption. *Industrial and Engineering Chemistry*, **1951**, *43* (6), 1460–1467.

54 W. E. Dobbins, in *Biological Treatment of Sewage and Industrial Wastes*, ed. M. L. McCable and W. W. Eckenfelder, Reinhold, New York, **1956**.

55 H. L. Toor and J. M. Marchello, Film-penetration model for mass and heat transfer. *AIChE Journal*, **1958**, *4* (1), 97–101.

56 G. Bercic and A. Pintar, The role of gas bubbles and liquid slug lengths on mass transport in the Taylor flow through capillaries. *Chemical Engineering Science*, **1997**, *52* (21–22), 3709–3719.

57 J. M. van Baten and R. Krishna, CFD simulations of mass transfer from Taylor bubbles rising in circular capillaries. *Chemical Engineering Science*, **2004**, *59* (12), 2535–2545.

58 C. O. Vandu, H. Liu and R. Krishna, Mass transfer from Taylor bubbles rising in single capillaries. *Chemical Engineering Science*, **2005**, *60* (22), 6430–6437.

59 R. Pohorecki, Effectiveness of interfacial area for mass transfer in two-phase flow in microreactors. *Chemical Engineering Science*, **2007**, *62* (22), 6495–6498.

60 J. D. Tice, H. Song, A. D. Lyon and R. F. Ismagilov, Formation of droplets and mixing in multiphase microfluidics at low values of the Reynolds and the capillary numbers. *Langmuir*, **2003**, *19* (22), 9127–9133.

61 J. R. Burns, J. N. Jamil and C. Ramshaw, Process intensification: operating characteristics of rotating packed beds – determination of liquid hold-up for a high-voidage structured packing. *Chemical Engineering Science*, **2000**, *55* (13), 2401–2415.

62 M. N. Kashid and D. W. Agar, Hydrodynamics of liquid–liquid slug flow capillary microreactor: flow regimes, slug size and pressure drop. *Chemical Engineering Journal*, **2007**, *131* (1–3), 1–13.

63 M. E. Charles, The pipeline flow of capsules (Part 2). *The Canadian Journal of Chemical Engineering*, **1963**, April, 46–51.

64 F. P. Bretherton, The motion of long bubbles in tubes. *Journal of Fluid Mechanics*, **1961**, *10* (2), 166–188.

65 M. N. Kashid, Experimental and modelling studies on liquid–liquid slug flow capillary microreactors, *PhD Thesis*, Technical University of Dortmund, **2007**.

66 G. Dummann, U. Quittmann, L. Groschel, D. W. Agar, O. Worz and K. Morgenschweis, The capillary-microreactor: a new reactor concept for the intensification of heat and mass transfer in liquid–liquid reactions. *Catalysis Today*, **2003**, *79* (1–4), 433–439.

67 J. R. Burns and C. Ramshaw, Development of a microreactor for chemical production. *Transactions of the Institution of Chemical Engineers*, **1999**, *77A*, 206–211.

68 J. R. Burns and C. Ramshaw, A microreactor for the nitration of benzene and toluene. *Chemical Engineering Communications*, **2002**, *189* (12), 1611–1628.

69 G. N. Doku, S. J. Haswell, T. McCreedy and G. M. Greenway, Electric field-induced mobilization of multiphase solution systems based on the nitration of benzene in a micro reactor. *Analyst*, **2001**, *126* (1), 14–20.

70 http://www.clarkson.edu/chemeng/faculty/jachuck.html.

71 O. Wörz, K. P. Jäckel, T. Richter and A. Wolf, Microreactors a new efficient tool for optimum reactor design, in *2nd International Conference on Microreaction Technology, New Orleans*, **1998**.

72 O. Wörz, K. P. Jäckel, T. Richter and A. Wolf, Microreactors a new efficient tool for optimum reactor design. *Chemical Engineering Science*, **2001**, *56* (3), 1029–1033.

73 B. Ahmed, D. Barrow and T. Wirth, Enhancement of reaction rates by segmented fluid flow in capillary scale reactors. *Advanced Synthesis and Catalysis*, **2006**, *348* (9), 1043–1048.

74 B. Ahmed-Omer, D. Barrow and T. Wirth, Effect of segmented fluid flow, sonication and phase transfer catalysis on biphasic reactions in capillary microreactors. *Chemical Engineering Journal*, **2007**, *135*, 280–283.

75 J. R. Burns and C. Ramshaw, The intensification of rapid reactions in multiphase systems using slug flow in capillaries. *Lab on a Chip*, **2001**, *1* (1), 10–15.

76 A.-L. Dessimoz, L. Cavin, A. Renken and L. Kiwi-Minsker, Liquid–liquid two-phase flow patterns and mass transfer characteristics in rectangular glass microreactors. *Chemical Engineering Science*, **2008**, *63*, 4035–4044.

77 J. Antes, D. Boskovic, H. Krause, S. Loebbecke, N. Lutz, T. Tuercke and W. Schweikert, Analysis and improvement of strong exothermic nitrations in microreactors. *Chemical Engineering Research and Design*, **2003**, *81*, (A7), 760–765.

78 K. Matsuyama, W. Tanthapanichakoon, N. Aoki and K. Mae, Operation of microfluidic liquid slug formation and slug design for kinetics measurement. *Chemical Engineering Science*, **2007**, *62*, (18–20 Special Issue), 5133–5136.

79 Z. T. Cygan, J. T. Cabral, K. L. Beers and E. J. Amis, Microfluidic platform for the generation of organic-phase microreactors. *Langmuir*, **2005**, *21* (8), 3629–3634.

80 A. Smirnova, K. Mawatari, A. Hibara, M. A. Proskurnin and T. Kitamori, Micro-multiphase laminar flows for the extraction and detection of carbaryl derivative. *Analytica Chimica Acta*, **2006**, *558* (1–2), 69–74.

81 T. Maruyama, J. Uchida, T. Ohkawa, T. Futami, K. Katayama, K. Nishizawa, K. Sotowa, F. Kubota, N. Kamiyaa and M. Goto, Enzymatic degradation of *p*-chlorophenol in a two-phase flow microchannel system. *Lab on a Chip*, **2003**, *3* (4), 308–312.

82 H. Song and R. F. Ismagilov, Millisecond kinetics on a microfluidic chip using nanoliters of reagents. *Journal of the American Chemical Society*, **2003**, *125* (47), 14613–14619.

83 M. Ueno, H. Hisamoto, T. Kitamori and S. Kobayashi, Phase-transfer alkylation reactions using microreactors. *Chemical Communications*, **2003**, 936–937.

84 M. N. Kashid, I. Gerlach, S. Goetz, J. Franzke, J. F. Acker, F. Platte, D. W. Agar and S. Turek, Internal circulation within the liquid slugs of a liquid–liquid slug-flow capillary microreactor. *Industrial and Engineering Chemistry Research*, **2005**, *44*, 5003–5010.

85 V. Hessel, P. Angeli, A. Gavriilidis and H. Lowe, Gas–liquid and gas–liquid–solid microstructured reactors: contacting principles and applications. *Industrial and Engineering Chemistry Research*, **2005**, *44* (25), 9750–9769.

86 M. W. Losey, R. J. Jackman, S. L. Firebaugh, M. A. Schmidt and K. F. Jensen, Design and fabrication of microfluidic devices for multiphase mixing and reaction. *Journal of Microelectromechanical Systems*, **2002**, *11* (6), 709–717.

87 M. W. Losey, M. A. Schmidt and K. F. Jensen, Microfabricated multiphase packed-bed reactors: characterization of mass transfer and reactions. *Industrial and Engineering Chemistry Research*, **2001**, *40* (12), 2555–2562.

88 K. K. Yeong, A. Gavriilidis, R. Zapf and V. Hessel, Catalyst preparation and deactivation issues for nitrobenzene hydrogenation in a microstructured

falling film reactor. *Catalysis Today*, **2003**, *81* (4), 641–651.

89 R. Födisch, D. Hönicke, Y. Xu and B. Platzer, Liquid phase hydrogenation of *p*-nitrotoluene in microchannel reactors, in *International Conference on Microreaction Technology (IMRET 5)*, Strasbourg, Springer, Berlin, **2001**.

90 M. W. Losey, M. A. Schmnidt and K. F. Jensen, A micro packed bed for chemical synthesis, in *International Conference on Microreaction Technology (IMRET 3)*, Frankfurt, Springer, Berlin, **2000**.

91 V. Hessel, W. Ehrfeld, T. Herweck, V. Haverkamp, H. Löwe, J. Schiewe, C. Wille, T. Kern and N. Lutz, Gas/liquid microreactors: hydrodynamics and mass transfer, in *Proceedings of the 4th International Conference on Microreaction Technology (IMRET 4)*, Atlanta, GA, **2000**.

92 K. K. Yeong, A. Gavriilidis, R. Zapf and V. Hessel, Experimental studies of nitrobenzene hydrogenation in a microstructured falling film reactor. *Chemical Engineering Science*, **2004**, *59* (16), 3491–3494.

93 C. De Bellefon, T. Lamouille, N. Pestre, F. Bornette, H. Pennemann, F. Neumann and V. Hessel, Asymmetric catalytic hydrogenations at micro-litre scale in a helicoidal single channel falling film micro-reactor. *Catalysis Today*, **2005**, *110* (1–2), 179–187.

94 D. A. Wenn, J. E. A. Shaw and B. Mackenzie, A mesh microcontactor for 2-phase reactions. *Lab on a Chip*, **2003**, *3* (3), 180–186.

95 R. Abdallah, P. Magnico, B. Fumey and C. De Bellefon, CFD and kinetic methods for mass transfer determination in a mesh microreactor. *AIChE Journal*, **2006**, *52* (6), 2230–2237.

96 M. T. Kreutzer, P. Du, J. J. Heiszwolf, F. Kapteijn and J. A. Moulijn, Mass transfer characteristics of three-phase monolith reactors. *Chemical Engineering Science*, **2001**, *56* (21–22), 6015–6023.

97 I. Aartun, B. Silberova, H. Venvik, P. Pfeifer, O. Görke, K. Schubert and A. Holmen, Hydrogen production from propane in Rh-impregnated metallic microchannel reactors and alumina foams. *Catalysis Today*, **2005**, *105* (3–4), 469–478.

98 D. van Herk, M. T. Kreutzer, M. Makkee and J. A. Moulijn, Scaling down trickle bed reactors. *Catalysis Today*, **2005**, *106* (1–4), 227–232.

99 S. Tadepalli, R. HaIder and A. Lawal, Catalytic hydrogenation of *o*-nitroanisole in a microreactor: reactor performance and kinetic studies. *Chemical Engineering Science*, **2007**, *62* (10), 2663–2678.

100 F. Trachsel, C. Hutter and P. R. von Rohr, Transparent silicon/glass microreactor for high-pressure and high-temperature reactions. *Chemical Engineering Journal*, **2008**, *135* (Suppl. 1), S309–S316.

101 R. Kaur, R. Machiraju and K. D. P. Nigam, Agitation effects in a gas–liquid–liquid reactor system: methyl ethyl ketazine production. *International Journal of Chemical Reactor Engineering*, **2007**, *5*, 1–19.

102 Y. Önal, M. Lucas and P. Claus, Application of a capillary microreactor for selective hydrogenation of α, β-unsaturated aldehydes in aqueous multiphase catalysis. *Chemical Engineering and Technology*, **2005**, *28* (9), 972–978.